Princeton Plasma Physics Laboratory

PPPL- 4690

PPPL- 4690

# Ideal MHD Stability and Performance of ITER Steady State Scenarios with ITBs

F.M. Poli, C.E. Kessel, M.S. Chance, S.C. Jardin and J. Manickam

September, 2011

PPPL PRINCETON PLASMA PHYSICS LABORATORY

Prepared for the U.S. Department of Energy under Contract DE-AC02-09CH11466.

# Princeton Plasma Physics Laboratory
# Report Disclaimers

---

## Full Legal Disclaimer



## Trademark Disclaimer



---

# PPPL Report Availability

## Princeton Plasma Physics Laboratory:

http://www.pppl.gov/techreports.cfm

## Office of Scientific and Technical Information (OSTI):

http://www.osti.gov/bridge

---

**Related Links:**

**U.S. Department of Energy**

**Office of Scientific and Technical Information**

**Fusion Links**

# Ideal MHD stability and performance of ITER steady state scenarios with ITBs

**F.M. Poli, C.E. Kessel, M.S. Chance, S.C. Jardin and J. Manickam**

Princeton Plasma Physics Laboratory, Princeton, NJ, 08543, USA.

**Abstract.** Non-inductive steady state scenarios on ITER will need to operate with Internal Transport Barriers (ITBs) in order to reach adequate fusion gain at typical currents of 9 MA. The large pressure gradients at the location of the internal barrier are conducive to the development of ideal MHD instabilities that may limit the plasma performance and lead to plasma disruptions. Fully non-inductive scenarios with five combinations of heating and current drive sources are presented in this work, with plasma currents in the range of 7 to 10 MA. For each configuration the linear, ideal MHD stability is analyzed for variations of the Greenwald fraction and of the pressure peaking factor around the operating point, aiming at defining an operational space for stable, steady state operations at optimized performance. It is shown that lower hybrid heating is desirable to maintain the safety factor profile above 1.5 and that these plasmas have better performance. Operating with moderate ITBs at 2/3 of the minor radius elevates the minimum safety factor above 2. This significantly improves stability and extends the operational space at normalized pressure above the ideal no-wall limit, although weak, residual large-n ballooning instabilities remain.

PACS numbers: 52.25,52.30,52.35,52.50,52.55,52.65

Submitted to: *Nuclear Fusion*

## 1. Introduction

ITER [1], the first fusion experiment to operate under reactor relevant conditions, will provide a unique opportunity to study burning plasma physics [2][3]. One of ITER's goals is to demonstrate feasibility of continuous operation using non-inductive current drive. Two candidates have been identified for advanced operations: the long duration, high neutron fluence hybrid scenario and the broad current steady state scenario [4]. The main characteristics and the physics challenges of both scenarios are reviewed by Joffrin [5], who discusses issues related to confinement and transport, stability and control of the current density and pressure profiles. These plasmas operate at a plasma current lower than the baseline configuration (the 15 MA ELMy H-mode inductive scenario) [6], to minimize the external heating power and current drive requirements [7]. The ITER steady state scenario targets plasmas with currents of 8-9 MA in the flat-top, with significant bootstrap current, self-generated by pressure gradients in magnetic field geometry [8]. Since the fraction of bootstrap current scales as $\beta_{\rm N} q_{95}$ [4], it is maximized at low current and high normalized pressure $\beta_{\rm N}$. Here $q_{95}$ is the safety factor at 95% of the poloidal flux surface and $\beta_{\rm N} = \beta(aB_0/I_{\rm P})$ [9], with $I_{\rm P}$[MA] the total current, $B_0$[T] the magnetic field, $a$[m] the minor radius and $\beta$ the ratio of the volume averaged plasma thermal energy to the magnetic energy. It has been estimated that, to compensate for the confinement degradation that occurs with decreasing plasma current and to get a fusion gain $Q = 5$ at a current of 9 MA, steady state operations should achieve $\beta_{\rm N} > 2.5$ with a confinement gain factor $H_{98} > 1.5$ [2][3][10]. This implies regimes with improved core confinement, or Internal Transport Barriers (ITBs) [11]. The large pressure gradients associated with ITBs in regions of weak or negative magnetic shear may drive ideal MHD instabilities in a wide range of $\beta_{\rm N}$, reducing the no-wall limits [12]. It is expected that steady state operations will be limited by the occurrence of resistive wall modes for pressure exceeding $\beta_{\rm N} = 4\ell_{\rm i}$ ($\ell_{\rm i}$ is the plasma internal inductance), necessitating a wall mode stabilization [5]. In addition, Alfvénic fast ion driven instabilities are more easily excited in plasmas with elevated safety factor in the core and $q_{\rm min} > 2$, typical of steady state scenarios [5][13].

Ideal $n = 1$ kink modes, driven by large pressure gradients at high $\beta_{\rm N}$, have led to disruptions on TFTR [14], JT-60U [15], JET [16][17], DIII-D [18] and ASDEX-U [19]. On the other hand, stable operations with $H_{98} \sim 1.6$, $\beta_{\rm N} \sim 2.5$, weak reversed magnetic shear, an internal transport barrier at $r/a \sim 3/4$, and with 70-80% of non-inductive current drive (1/3 NB and 2/3 bootstrap) have been demonstrated on JT-60U [20]. Both theory and experiments have shown that the $\beta_{\rm N}$ limit imposed by the $n = 1$ ideal kink can be improved by operating with broader pressure profiles [15][16][18][21], although a consistent improvement (namely $\beta_{\rm N} = 3.5 - 4.0$ with $p(0)/\langle p \rangle \sim 3$) can be obtained only with strongly shaped plasmas, at triangularity $\delta \gtrsim 0.7$ [12][22][23].

In this work, we examine steady state configurations with ITBs, plasma currents in the range of 7-10 MA, densities of 0.85-1.0 of the Greenwald density $n_{\rm G}$ and with five different combinations of heating and current drive sources, namely negative ions

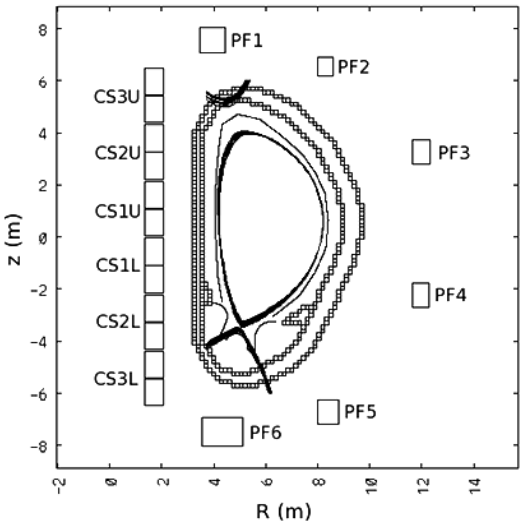


**Figure 1.** Sketch of the ITER vacuum vessel and conducting structures, the central solenoid and poloidal field coils included in TSC. Also shown is the separatrix surface at a few time slices during the stationary current flat-top phase.

neutral beam, ion and electron cyclotron and lower hybrid current drive (Sec.3). These configurations are established as relaxed flat-top states with time-dependent transport simulations. For each heating configuration we analyze the ideal MHD stability to $n = 1, 2$ kink and to $n = \infty$ ballooning modes (Sec.3.2), the sensitivity of stability to variations of the pressure profile peaking and of the Greenwald fraction (Sec.4) and discuss the operational limits (Sec.6). It will be shown that configurations with lower hybrid heating are more likely to maintain the minimum safety factor above 1.5, which is desirable in steady state operations to avoid $(3, 2)$ Neoclassical Tearing Modes. When operating at $q_{\min} > 2$, which can be obtained with broad pressure profiles and ITBs at 2/3 of the minor radius, these plasmas can achieve $\beta_{\rm N} \gtrsim 4\ell_i$ with an ideal wall, as discussed in Sec.6.

## 2. Scenario development

### *2.1. Computational models*

Full plasma discharges are simulated with the Tokamak Simulation Code (TSC) [24], a predictive, free boundary transport evolution code that solves the 2D axisymmetric Maxwell-MHD equations on a $(R, Z)$ grid, coupled to 1D flux surface averaged transport equations for energy and particles. The TSC includes a 2D representation of the central solenoid and of the poloidal field coils, of the surrounding conducting structures and feedback systems for plasma position, shape and current (see Fig.1).

There are several additional physics models that are used in the simulations such as bootstrap current and radiation, which are described in Sec.2.2. TSC is used to establish

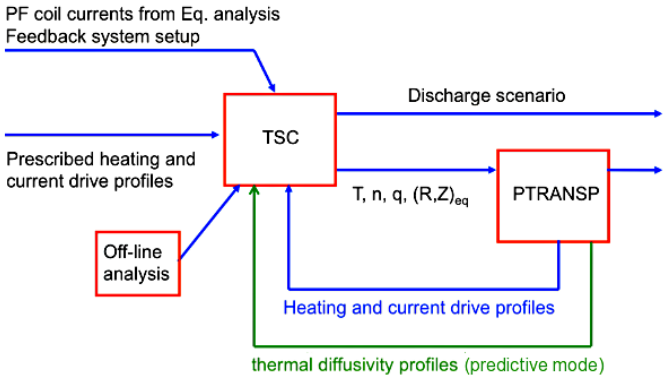


**Figure 2.** (Colour online) Schematic of the TSC/TRANSP computational loop. In analysis mode only the heating and current drive profiles from TRANSP are used by TSC, while in predictive mode also the thermal diffusivities profiles are used.

the scenario in terms of all parameters as a function of time, targeting the desired properties of the scenario and attempting to remain within all limits. The TRANSP [25] code is a prescribed boundary transport evolution code, extensively used in tokamak experimental interpretation, and possesses high fidelity models for heating and current drive sources and fast particle accounting. This code also has several additional physics models available for integrated simulations. In addition, predictive simulations are possible in TRANSP given sufficient information on the plasma boundary and other time-dependent parameters. The relationship between TSC and TRANSP in computing scenarios can take one of two forms: an analysis mode or a predictive mode. In this work TRANSP is used in analysis mode, with TSC providing experimental like conditions: the plasma boundary, the density, temperature and impurities profiles, the total plasma current are input to TRANSP, which calculates the heating and current drive deposition profiles. These are then given back to TSC in analytic form for re-calculation of the scenario, reducing considerably the computational time. This approach is particularly suited for steady state development, where one needs to align the plasma and the non-inductive current by adjusting the thermal diffusivity and the pedestal height. A schematic of the computational flow between TSC and TRANSP is illustrated in Fig.2. In the predictive mode, only the plasma boundary and global scalar time history data are preserved, while TRANSP calculates its own 1D transport for the temperature, density, momentum and current.

### *2.2. Primary physics models and scenario assumptions*

Various physics models are used in the analysis of scenarios for ITER, and there are also a number of assumptions built into the discharges, the most important of which are outlined in this section.

All simulations begin with a large bore 500 kA plasma, which is grown to full size and shape by $\sim$ 14 s, at which time the X-point forms and the plasma is diverted, at

**Table 1.** Plasma parameters for the five reference scenarios shown in Fig.4, calculated at $t = 2000\,\mathrm{s}$. The toroidal magnetic field is $B_0 = 5.3\,\mathrm{T}$ in all cases. The shot number refers to the TRANSP run. Quantities in bold fonts are input to TSC, like the central density $n(0)$, the density peaking factor $n(0)/\langle n\rangle$, the ITB foot location $\rho_{\mathrm{ITB}}$ and the requested plasma current waveform $I_{\mathrm{P}}$.

| SHOT# | 31001 | 32001 | 33001 | 34001 | 35001 |
|---|---|---|---|---|---|
| NB (MW) | 33 | 33 | 33 | 33 | 8 |
| IC (MW) | 20 | 20 | / | 20 | 20 |
| EC (MW) | 20 | 40 | 20 | / | / |
| LH (MW) | / | / | 20 | 40 | 40 |
| **$\mathbf{I_p}$ (MA)** | 7.0 | 9.0 | 8.85 | 10.0 | 7.25 |
| $I_{\mathrm{NI}}$ (MA) | 7.04 | 9.09 | 8.90 | 10.20 | 7.5 |
| $I_{\mathrm{BS}}$ (MA) | 3.4 | 3.8 | 4.8 | 5.2 | 4.9 |
| $I_{\mathrm{NB}}$ (MA) | 2.6 | 3.1 | 2.4 | 2.8 | 0.56 |
| $I_{\mathrm{EC}}$ (MA) | 0.74 | 1.66 | 0.73 | / | / |
| $I_{\mathrm{IC}}$ (MA) | 0.25 | 0.40 | / | 0.25 | 0.25 |
| $I_{\mathrm{LH}}$ (MA) | / | / | 0.83 | 1.8 | 1.75 |
| $f_{\mathrm{BS}}$ | 0.48 | 0.41 | 0.54 | 0.51 | 0.65 |
| $P_\alpha$ | 28 | 52 | 64 | 76 | 33 |
| $Q$ | 2.4 | 3.3 | 4.3 | 4.9 | 2.4 |
| $P_{rad}$ | 22 | 31 | 35 | 38 | 27 |
| $n/n_G$ | 1.00 | 0.86 | 0.95 | 0.85 | 1.0 |
| $\mathbf{n(0)[10^{19}m^{-3}]}$ | 7.0 | 7.5 | 8.5 | 8.7 | 7.2 |
| $T(0)$ (keV) | 19 | 32 | 25 | 32 | 18 |
| $\mathbf{n(0)}/\langle\mathbf{n}\rangle$ | 1.44 | 1.4 | 1.44 | 1.5 | 1.3 |
| $p(0)/\langle p\rangle$ | 2.63 | 2.56 | 2.6 | 2.90 | 2.33 |
| $\rho_{\mathbf{ITB}}$ | 0.55 | 0.55 | 0.65 | 0.45 | 0.65 |
| $l_i(1)$ | 1.07 | 1.22 | 0.85 | 0.80 | 0.58 |
| $l_i(3)$ | 0.87 | 1.00 | 0.69 | 0.66 | 0.48 |
| $H_{98}$ | 1.55 | 1.58 | 1.63 | 1.63 | 1.55 |
| $q(0)$ | 1.61 | 1.67 | 3.3 | 1.88 | 6.05 |
| $q_{min}$ | 1.35 | 0.96 | 1.71 | 1.67 | 4.5 |
| $q_{95}$ | 7.0 | 5.4 | 5.2 | 4.7 | 6.78 |
| $\beta_{\mathrm{N}}$ | 2.0 | 2.4 | 2.6 | 2.7 | 2.13 |
| Ballooning | S | S | U | U | S |
| $n = 1$, no wall | S | U | S | U | S |
| $n = 1$, wall | S | U | S | S | S |

$I_{\mathrm{P}} = 3\,\mathrm{MA}$. All plasmas have the same target geometry of $R = 6.2$ m, $a = 2.0$ m, elongation $\kappa \sim 1.8$ and triangularity $\delta \sim 0.45$.

The pedestal is modeled with EPED1 [26], a peeling-ballooning ideal MHD stability model. Within the range of plasma currents accessed, $I_{\rm P} = 7 - 10$ MA, and densities required, $n_0 \sim (7.0 - 8.5) \times 10^{19}\,{\rm m}^{-3}$ (with $n_{\rm ped} \sim (4.0 - 5.0) \times 10^{19}\,{\rm m}^{-3}$ at $\rho_{\rm ped} \sim 0.94$), the pedestal temperature is predicted to be $T_{\rm ped} = 3.3 - 3.7\,{\rm keV}$. All simulations presented herein aim at keeping $T_{\rm ped}$ within this window. Since transport models used for H-mode plasmas (like the baseline and the hybrid scenarios) that are dominated by $\mathbf{E} \times \mathbf{B}$ rotational shear stabilization have deficiencies when applied to reversed shear plasmas and high pressures [27], no first principle transport model is used in this work. Instead, a semi-empirical approach is adopted to produce an ITB in the electron and ion temperature through a modified thermal diffusivity profile: a combination of an L-mode Coppi-Tang model for the interior region [28] and two terms to model, respectively, the ITB foot and the pedestal [7]. The ITB foot location, $\rho_{\rm ITB}$, is defined as the location of minimum thermal diffusivity. A target global energy confinement time multiplier of $H_{98} \sim 1.6$ is found to be necessary to obtain both 100% non-inductive current in the above range and a plasma fusion gain of 3-5 [29].

The electron density profile and magnitude are prescribed, with a peaking factor of $n(0)/\langle n \rangle = 1.3 - 1.5$ in the H-mode phase assumed in this work. The Helium concentration is determined by an input $\tau^*_{\rm He}/\tau_{\rm E} = 5$ and includes the buildup to burn conditions. The Hydrogen (DT) fuel density is determined from quasi-neutrality assuming equal amounts of D and T. The impurity density profiles are assumed to be the same as the electron density, with their fractions prescribed as a function of time. Radiation includes bremsstrahlung, cyclotron (Trubnikov model), and line (coronal equilibrium).

The plasma configurations must be consistent with the power and particle handling in the divertor. Although scrape-off layer plasma and neutral particle analysis are not done as part of these time-dependent calculations, all scenarios are attempting to elevate the radiated power from the core plasma in order to keep the conducted power to the divertor in the proper range [30]. It is assumed a 2% concentration of Berillium and 0.4% of Argon (0.01% in L-mode), which provide 25-45 MW of core radiated power, depending on the scenario, and brings the conducted power to the divertor to 80-100 MW.

### *2.3. Heating and Current Drive Sources*

The steady state scenario is significantly dependent on the heating and current drive sources, since the current deposition profiles, in combination with the bootstrap current, determine the safety factor profile. The external power heating sources considered herein are 33 MW of neutral beam (NB), 20 MW of ion cyclotron (IC), 20-40 MW of electron cyclotron (EC), and 20-40 MW of lower hybrid (LH). Each of the sources have defined parameters such as frequency, particle energy, spectra, and steering angle. The frequency of the IC and the steering angles for the NB and EC used in this work are based on previous optimization studies of the total driven current [29][31].

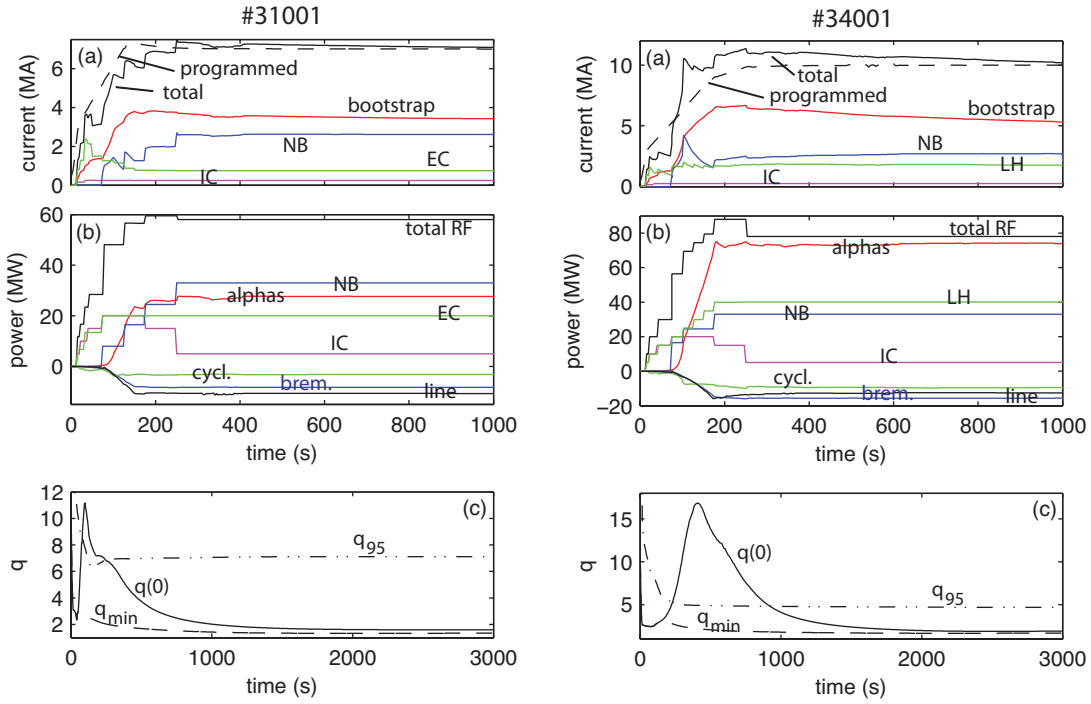


**Figure 3.** (Colour online) Left: day one heating mix scenario (33MW NB+20MW IC+20MW EC). Right: scenario with 33MW NB+20MW IC + 40MW LH. (a) time history of bootstrap and RF driven current, of requested (dashed) and total non-inductive (black) current; (b) external, radiated and alpha's power; (c) evolution of the safety factor on axis $q(0)$, at the minimum ($q_{\rm min}$) and at 95% of the poloidal flux ($q_{95}$). The full time scale is shown here.

The alpha particle source models are an orbit following Monte Carlo and Bosch-Hale reactivity formulation. The ICRF source model is the TORIC full wave [32] with a Fokker Planck treatment of the resonant species and equivalent Maxwellians for other fast species (neutral beam ion and alpha particles). A frequency of 48 MHz is used here to obtain on-axis deposition and to accommodate the strong magnetic axis shift; a FWCD component of $\sim 200-400\,$kA on axis is taken for 20 MW of IC, estimated by scaling from CURRAY ray-tracing analysis [7]. The NB source model is the NUBEAM orbit following Monte Carlo [33][34]. The NB has 1 MeV particle energy, with the capability to steer from on-axis to off-axis. Full off-axis steering is used here, which can deliver up to $\sim 3\,$MA of non-inductive current with deposition peaked at $\rho \sim 0.3-0.35$, at full power of 33 MW ($\rho$ is defined as the squared root of the normalized toroidal flux). The lower hybrid model is the ray-tracing 1D Fokker Planck LSC code [35], augmented with a correction factor ($\times 1.6$) based on comparisons with GENRAY/CQL3D ray-tracing 2D Fokker Planck model [36]. The LH spectrum is peaked at $n_{\|} = 2.15$ and -3.9, with $\Delta n_{\|} = 0.2$, and with 87% forward and 13% backward power weighting (which provides the factor of 1.6 enhancement in the total driven current, compared to the reference weighting 72.5% forward and 27.5% backward). The electron cyclotron model

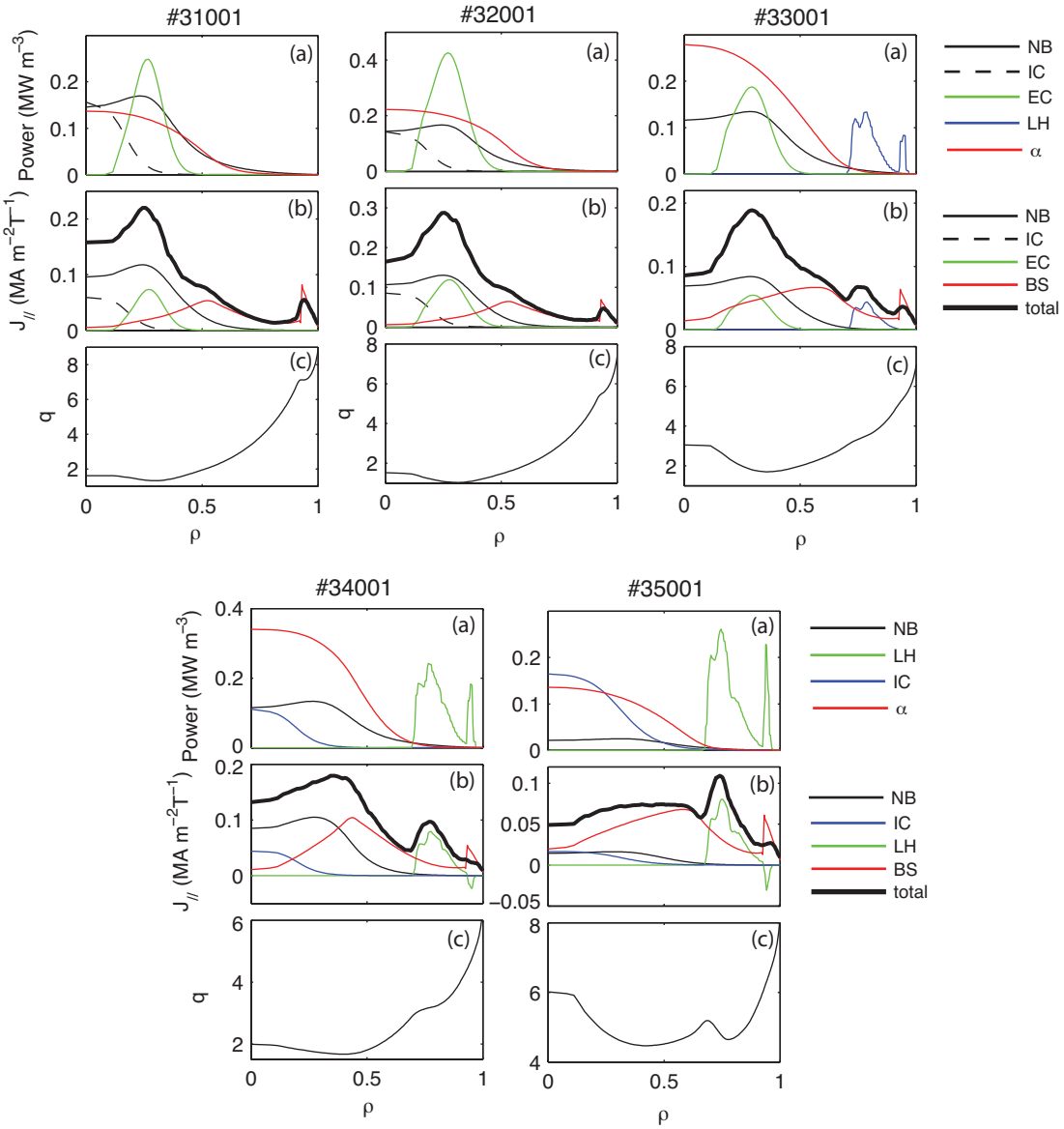


**Figure 4.** (Colour online) (a) Power density deposition profiles, (b) current density profiles, (c) safety factor profile for the five reference scenarios, calculated at $t = 2000$s.

is the ray-tracing 1D Fokker Planck TORAY code [37][38]. With steering angles of 40° (lower), 38° (middle), and 38° (upper), the EC power deposition peaks at $\rho \sim 0.35$, giving 0.7 MW of current drive for 20 MW of injected power. It should be noted that the ECRH design in ITER has been modified so that only 2 of the equatorial launchers can inject in the co-current direction. The current drive predictions shown here assuming that all three launchers can inject in the co-current direction are therefore optimistic by the ratio of 13.4/20.

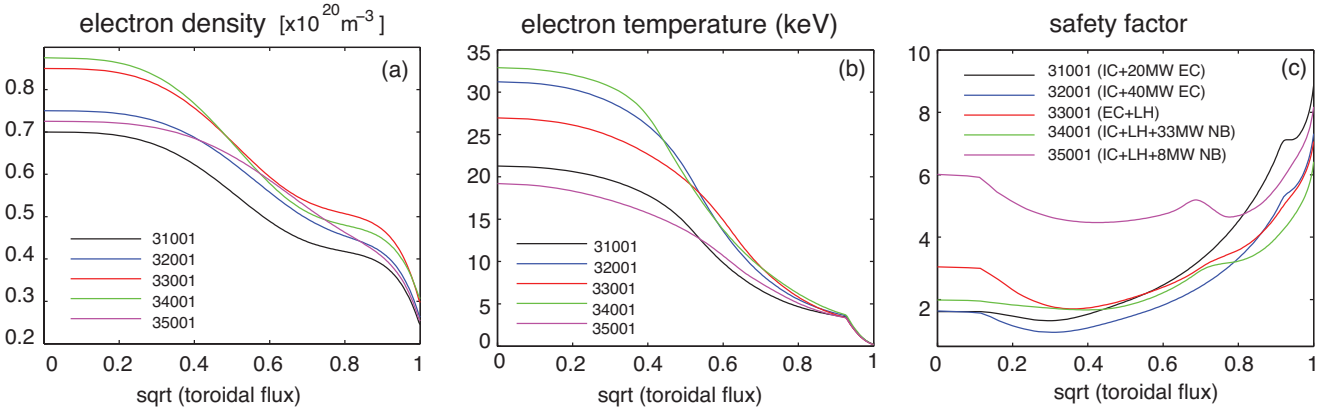


**Figure 5.** (Colour online) Profiles of electron density (note the suppressed zero) (a), electron temperature (b) and safety factor (c), calculated at $t = 2000\,\mathrm{s}$, for the five reference scenarios listed in Table 1.

### *2.4. Ideal MHD stability calculations*

The flattop plasma solutions calculated with TSC are refined with JSOLVER [39], a fixed-boundary, single fluid, flux-coordinate equilibrium solver. The cartesian coordinates $(R, Z)$ are treated as functions of the poloidal flux $\psi$ and poloidal angle $\theta$ and are iterated on until they satisfy a second-order finite difference approximation to the Grad-Shafranov equation. The $(R, Z)$ are constrained to form a coordinate system with an equal arc-length Jacobian: the poloidal arc-length subtended per radian of poloidal angle is constant on a flux surface. For the stability studies presented herein, a grid of $257 \times 256$ points in $(\psi, \theta)$ is used for the equilibrium reconstruction. The stability against linear kink modes is studied with PEST-I (Princeton Equilibrium and STability) [40], a suite of codes that determine the linear stability of an axisymmetric toroidal plasma using the ideal MHD theory. The PEST-I code determines the stability of a given equilibrium using the $\delta W$ method.

Stability against large toroidal mode number ballooning instabilities is studied with BALMSC [41]. First, the Mercier condition for stability of localized modes is solved [42]; then, if the equilibrium is stable to Mercier, BALMSC solves the ballooning eigenvalue equation in the large toroidal mode number approximation on each flux surface.

## 3. Reference scenarios

The scenarios analyzed include the 2004 baseline configuration with total external power of 73 MW [43], consisting of 33 MW of NB and 20 MW each of EC and IC heating (hereafter day-one heating mix scenario), as well as four upgrade scenarios with various combinations of NB, IC, EC and LH. These include two variations of the day-one heating mix configuration, one with 40 MW of EC, the other with 20 MW of IC replaced by 20 MW of LH, as well as two scenarios with 20 MW of IC and 40 MW of LH, respectively with additional 33 MW and 8 MW of NB. All these scenarios are based

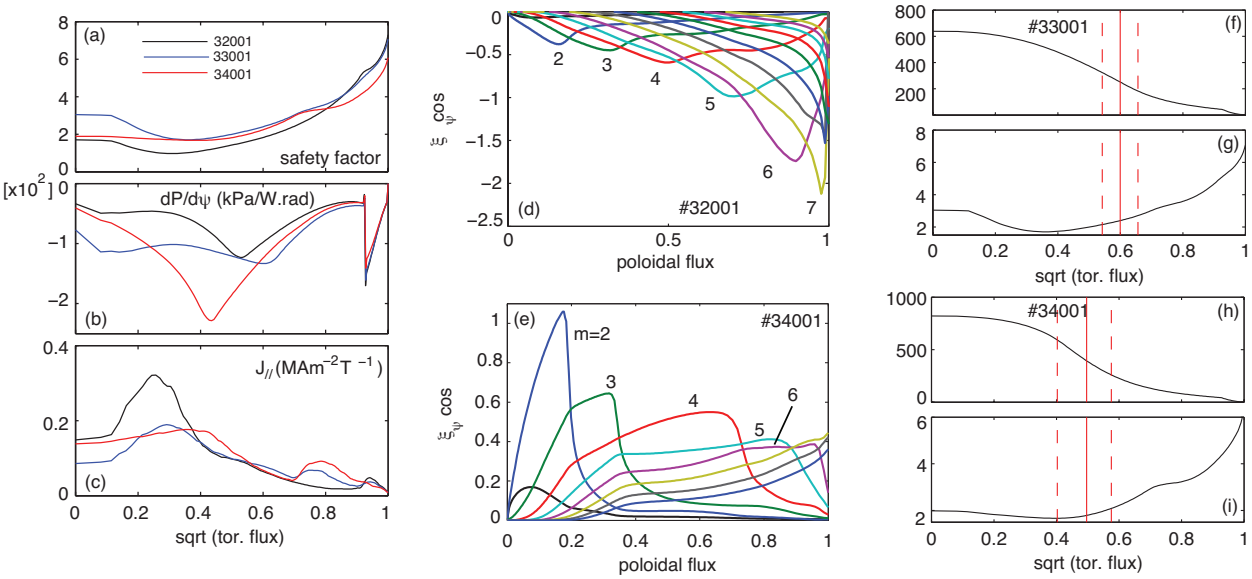


**Figure 6.** (Colour online) Summary of the ideal MHD stability analysis for the reference cases. Left column: safety factor (a), pressure derivative (b) and parallel current (c) profiles for the unstable cases. Middle column: Fourier components of the $n = 1$ kink for the scenarios with 40 MW EC (d) and with 40 MW LH (e). Right column: pressure and $q$ profiles for the two scenarios ballooning unstable, #33001 and #34001. The vertical red line indicates the location of maximum ballooning instability amplitude, while the two dashed lines mark the radial extension of the unstable region.

on the configurations presented in ref. [29]. They have the same heating and current drive combination of sources and the same central density, but use more converged calculations of the EC and NB deposition profiles and current drive from TRANSP; the total plasma current may therefore differ from the previous simulations in some cases. The ramp-up phase duration is fixed at 150 s and the whole 3000 s flattop burning phase is simulated to allow complete current profile relaxation and to study the MHD stability as the $q$ profile evolves. The current ramp-down phase is not considered in this work that aims at identifying a range of ideal MHD stable equilibria in flattop conditions.

### *3.1. Plasma parameters*

The main plasma parameters and the heating and current drive sources of the five reference scenarios are summarized in Table 1; the power deposition profiles are shown in Fig.4 while the profiles of electron density, temperature and safety factor are compared in Fig.5. All profiles shown are calculated at about 2/3 of the current flat-top phase, after the current profiles have relaxed and the loop voltage has become stationary.

The plasma current spans from 7 to 10 MA, with fully non-inductive current driven in the flat-top in all cases and a bootstrap fraction of 65% in the plasma with 8 MW of NB and about 40-50% in the other cases. The bootstrap model used here is the Sauter model [44]; compared with the NCLASS module [45] in TRANSP, the predicted current

varies between 1-2% in the scenarios with IC and EC heating to 3-4% in those with EC and LH heating and with 8 MW NB. The largest difference is found in the scenario with $I_P = 10\,\mathrm{MA}$, where the Sauter model predicts a 10% higher bootstrap current compared to NCLASS.

The H/CD begins just after the divert time with significant power levels ramping up to drive non-inductive current approaching the total plasma current. The IC, LH and EC sources are used in the earliest phase of the current ramp-up and continue through the discharge, while the NB are used only after the permissible density is reached (approximately half way through the ramp-up). In all the scenarios with 33 MW of NB the IC power is stepped-down from 20 MW to 5 MW early in the flat-top; the IC source is needed in fact only to drive current in the core and prevent the formation of a current hole and $q$ to reach very high values on axis.

The current ramp-up time is kept fixed at 150 s to avoid injecting too much inductive current. It is also found that driving excessive non-inductive current in the ramp-up phase leads to large values of $q$ on axis and to long relaxation times [29]. The negative loop voltage provided by the central solenoid (CS) and poloidal field (PF) coils, in response to this non-inductive current over-drive, is driven at the plasma edge, and diffuses into the core over the long current diffusion time-scale, resulting in a suppression of current density and elevation of $q(0)$. An example is shown in Fig.3 for two cases: the 7 MA configuration with 20 MW of EC and IC (#31001) and the 10 MA scenario with 40 MW of LH and 33 MW of NB (#34001). In the latter case, where the NB is stepped-up to full power earlier because of the higher density, $q(0)$ reaches larger values and relaxes to stationary values over longer time scales. This can be avoided by keeping the total non-inductive current below the requested total plasma current value during the ramp-up phase and letting the ohmic current assist until the start of the burning phase [29]. However, the balance of enough power to drive current and to enter the H-mode requires some optimization, since entering the H-mode with confidence usually requires using total power exceeding the threshold by a factor of 1.5-2, while such powers can also drive excessive current at the low densities where the L to H transition is desired.

The current profile is dominated by the NB driven current (see Fig.4), which is an efficient source and deposits close to the magnetic axis. The narrower deposition of EC largely adds to the broader NB current profile around $\rho = 0.35$. In the configuration with 40 MW of EC, the peaked current profile at this location causes the minimum safety factor to drop below unity in the relaxed phase.

Although 40 MW of LH can drive almost 1.8 MA of current, this heating source can raise the value of $q_{\min}$, but cannot control its location unless the NB power is reduced (cases #34001 and #35001). The safety factor profile features in the configuration with lower NB power are mainly from the LH and from the bootstrap current and LH is competitive in shaping this profile.

Central densities are in the range of $(7 - 8.7) \times 10^{19}\,\mathrm{m}^{-3}$, which correspond to a Greenwald fraction of 0.85 at the largest current and of 1.0 at the lowest. The scenario with 33 MW of NB, IC and LH (#34001) has the largest normalized pressure,

$\beta_N = 2.7$, and fusion gain, $Q \simeq 5$. This plasma also has the highest pressure, with central temperature above 30 keV and density $8.7 \times 10^{19}\,\mathrm{m}^{-3}$, and the most peaked pressure profile, with $p(0)/\langle p\rangle = 2.98$ compared to $p(0)/\langle p\rangle = 2.30$ for the same combination of IC+LH at lower beam power, and about 2.6 for the three scenarios with EC heating. The pedestal temperature is comparable in all cases and it is $T_{\mathrm{ped}} \simeq 3.6 - 3.7\,\mathrm{keV}$ (see Fig.5-b).

All plasmas maintain a magnetic shear profile reversed in the core also at the end of the burning phase, as shown in Fig.5c, encompassing configurations with weak shear, like the two scenarios with IC and EC heating, and almost no-shear (plasma with IC, LH and 33 MW of NB) to moderate shear as in the plasmas with EC and LH and with 8 MW of NB. The minimum safety factor is above 1.5 in the three configurations with LH heating, and below 1.5 in the two configurations with IC and EC heating.

### *3.2. Ideal MHD stability*

The results of the ideal MHD stability analysis for the five reference cases, calculated after current profile relaxation and with a wall at infinity, are summarized in Table 1.

The scenario with 8 MW of NB (#35001) and the day-one heating mix (#31001), both with low plasma current and low $\beta_N$, are ideal MHD stable. The low $\beta_N$ achieved makes #31001 stable to $n = 2$ kinks even with $q_{\min} < 1.5$.

Adding 20 MW EC to the day-one heating mix configuration improves the performance, raising $Q$ from 2.4 to 3.3 and $\beta_N$ from 2.0 to 2.4 (see Table 1, shot #32001). However, the localized current drive from EC and NB results in a peaked current profile and causes the minimum safety factor to drop below unity. The relaxed equilibrium is unstable to ideal kinks with $n = 1$ and $n = 2$. On surfaces where $q_{\min} = 1.5$, and where $q_{\min} = 1.0$ the Mercier criterion for localized instabilities is also violated. Figure 6-d shows the Fourier components of the $n = 1$ kink mode, calculated with the conducting wall at infinity. It is found that the conforming wall (modeled at $a_w/a - 1 = 0.35$ for $a = 2$m and $R = 6.2$m [12]) can only reduce the amplitude of the modes, but cannot effectively stabilize them.

Replacing IC with LH in the day-one heating mix configuration (#33001), while keeping the same EC power, improves both performance and ideal MHD stability. The safety factor is raised above 1.5, as shown in Table 1 and in Fig.6-a, and, with slightly lower non-inductive current than the configuration with 40 MW EC (#32001), this plasma can achieve $\beta_N = 2.6$ and fusion gain about 35% larger. The relaxed equilibrium is stable to ideal kink modes in the flat-top, but is unstable to ballooning modes with $n > 37$. The most unstable region is outside $q_{\min}$, where $q = 2.4$ and the ITB pressure gradient is maximum (see Fig.6-f,g). However, this region has limited radial and poloidal extent, suggesting that these large $n$ ballooning instabilities may not be harmful to the plasma.

The heating mix configuration with 33 MW of NB and 40 MW LH (#34001) has the most peaked pressure profile, with $n(0)/\langle n\rangle = 1.5$ and ITB foot at $\rho_{\mathrm{ITB}} = 0.45$,

and the largest normalized pressure, $\beta_N = 2.7$. The relaxed equilibrium is unstable to $n > 17$ ballooning and to $n = 1$ kink instabilities. The ballooning unstable region has radial extent of 18%, is extended poloidally and has its maximum amplitude at $q = 1.8$, close to $q_{min}$ (see Fig.6-i). A dominant $m = 2$ component is present in the spectrum of the $n = 1$ kink, as shown in Fig.6-(e), and harmonics with $m > 4$ have comparable amplitude. The mode structure is similar to the so-called 'infernal' mode, an ideal $n = 1$ kink instability driven at large $\beta_N$ primarily by the pressure gradient in the low shear region, which develops close to the minimum of the safety factor profile [46].
We note that similar spectra have been observed prior to disruptive termination of the plasma in several tokamaks, including JT-60U [15], although operations with ITBs at high $\beta_N$ have been demonstrated possible on the same device [20].

**Table 2.** Scenarios with 20MW IC and 20MW EC heating. Variations of the reference scenario #31001 for different values of the pressure peaking around the operating point, at the same current and at larger current (columns 1 to 4). The last three columns refer to cases with higher central temperature and higher non-inductive current. The shot numbers refer to the TRANSP run. Input parameters to TSC are indicated in bold fonts. All cases are ideal MHD stable.

| 33 MW NB<br>20 MW IC<br>20 MW EC | 31021 | 31033 | 31032 | 31011 | 31501 | 31521 | 31511 |
|---|---|---|---|---|---|---|---|
| $\mathbf{I_P}$ **(MA)** | 7.0 | 7.0 | 7.0 | 7.0 | 7.4 | 7.4 | 7.4 |
| $I_{NI}$ (MA) | 7.05 | 6.95 | 7.03 | 6.99 | 7.42 | 7.37 | 7.39 |
| $I_{NB}$ (MA) | 2.45 | 2.6 | 2.5 | 2.3 | 2.8 | 2.6 | 2.5 |
| $I_{BS}$ (MA) | 3.6 | 3.2 | 3.5 | 3.7 | 3.5 | 3.6 | 3.9 |
| $I_{EC}$ (MA) | 0.72 | 0.79 | 0.70 | 0.69 | 0.80 | 0.78 | 0.76 |
| $P_\alpha$ | 31.0 | 29 | 28 | 33 | 34 | 37 | 41 |
| $Q$ | 2.67 | 2.5 | 2.4 | 2.9 | 2.9 | 3.2 | 3.6 |
| $p(0)/\langle p\rangle$ | 2.47 | 2.87 | 2.5 | 2.6 | 2.67 | 2.49 | 2.6 |
| $\mathbf{n(0)/\langle n\rangle}$ | 1.34 | 1.44 | 1.44 | 1.44 | 1.44 | 1.34 | 1.44 |
| $\mathbf{n(0)[10^{19}m^{-3}]}$ | 7.0 | 7.0 | 7.0 | 7.7 | 7.0 | 7.0 | 7.7 |
| $T_e(0)$ (keV) | 21 | 23 | 21 | 21 | 24 | 24 | 23 |
| $\rho_{\mathbf{ITB}}$ | 0.55 | 0.45 | 0.65 | 0.55 | 0.55 | 0.55 | 0.55 |
| $\beta_N$ | 2.18 | 2.07 | 2.07 | 2.22 | 2.36 | 2.1 | 2.3 |
| $q(0)$ | 1.67 | 1.47 | 1.64 | 1.80 | 1.69 | 1.49 | 1.48 |
| $q_{min}$ | 1.43 | 1.21 | 1.38 | 1.50 | 1.36 | 1.23 | 1.24 |
| $H_{98}$ | 1.61 | 1.55 | 1.57 | 1.61 | 1.66 | 1.59 | 1.64 |
| $n/n_G$ | 1.0 | 1.0 | 1.0 | 1.1 | 1.05 | 0.94 | 0.99 |

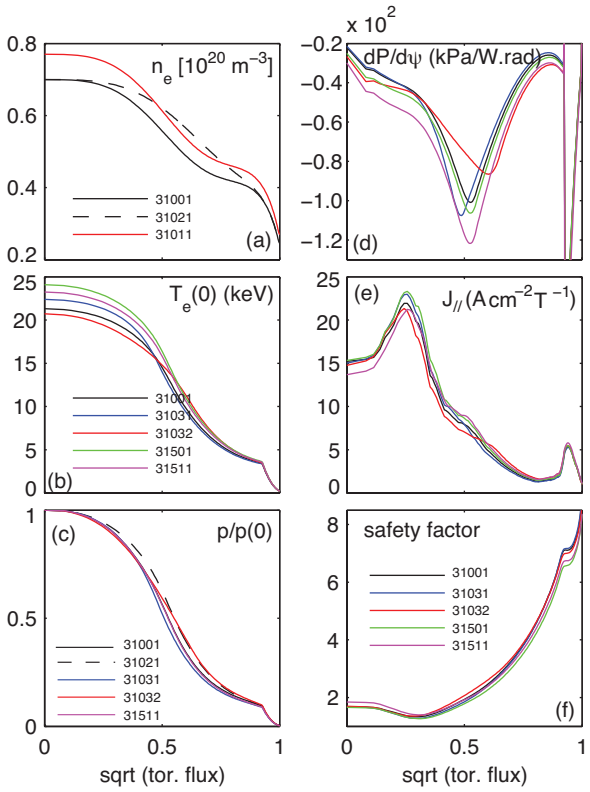


**Figure 7.** (Colour online) Scenarios with 20 MW IC and 20MW EC. (a) Density profiles for the cases with $n(0)/\langle n\rangle = 1.44$ (#31001), $n(0)/\langle n\rangle = 1.3$ (#31021) and $n(0)/\langle n\rangle = 1.5$ and $n = 1.1n_{\rm G}$ (#31011). All other cases use these density profiles. (b) Temperature profiles. (c) pressure profiles, normalized to the maximum. (d) pressure derivative. (e) total parallel current. (f) safety factor profiles.

## 4. Ideal MHD stability around the operating point

We have analyzed the ideal MHD stability of the above configurations about the operating point, for perturbations of approximately 10% in the Greenwald fraction and in the density and temperature peaking factor. When one of the parameters is modified, the others are kept fixed, aiming at recovering the non-inductive current achieved in the corresponding reference cases. However, perturbations in the various quantities should be expected, since - when one parameter is changed - the plasma equilibrium, the bootstrap response and the heating and current drive sources are re-calculated self-consistently.

The pressure peaking profile can be modified either through the analytic form of the density profiles or by moving the ITB foot location. Both approaches are separately undertaken, with density peaking varied in the range of 1.3-1.5 and ITB foots between 1/2 and 3/4 of the minor radius.

For each heating mix configuration we discuss the ideal MHD stability when the above parameters are varied, then we find the stability limits by exploring configurations at larger pressure, but still having densities less than $\sim 1.2n_{\rm G}$. It will be shown that

plasmas where LH is combined either with EC or IC have larger minimum safety factor values and better performance compared to plasmas with a mix of IC and EC heating. This section focusses on the stability of relaxed equilibria, while Sec.5 will discuss the MHD stability of the same configurations in the flat-top, before current profile relaxation.

### *4.1. Configurations with 33 MW NB, 20MW IC and 20MW EC*

This configuration maintains good MHD stability around the operating point. Table 2 summarizes the results for some of the configurations explored, while Fig.7 shows the profiles of $q$, electron density and temperature, total current density and pressure derivative.

Although the $q = 1.5$ rational surface is left inside the plasma, equilibria are found to be stable against $n = 2$ ideal kinks at this pressure. The minimum safety factor can be raised either operating with broader pressure profiles or increasing the density by 10% (#31011). The reduced current drive efficiency lowers the maximum current at the NB and EC deposition radius, while the higher bootstrap current raises the current off-axis, resulting in broader current and $q$ profiles. For the small perturbations of the pressure peaking factor considered in this work, variations in the current drive efficiency are usually compensated by an opposite variation of the bootstrap current.

As shown in table 2, a current of 7 MA is achieved within 50kA both for broader (#31021 and #31032) and more peaked (#31033) pressure profiles and for densities 10% larger (#31011). With comparable pressure peaking factor, operating with broader density profiles results in a better performance than operating with broader ITBs, although the improvement in the fusion gain is barely 10%.

Since the current drive efficiency scales with $T(0)n^{-1}$, increasing the central temperature at constant density increases the externally driven current. We have studied scenarios with the same heating mix but higher temperature and thus higher non-inductive current.

Table 2 reports three cases (last three columns): one with the same density profile as the reference scenario (#31501), one with broader density profile (#31521) and one with density raised by 10% (#31511). These three configurations have respectively the same density profiles as #31001, #31021 and #31011, but larger current and temperature, and operate at lower Greenwald fractions. Compared to the reference scenario at 7.0 MA (#31001), #31501 has higher fusion gain factor and higher $\beta_{\rm N}$, but lower minimum safety factor (1.23 compared to 1.35) because of the larger non-inductive current. If the density is increased by 10%, bringing the Greenwald fraction to 1.0 (#31511), the fusion gain increases to 3.6.

It should be noted that the target global confinement factor of $H_{98} \simeq 1.6$ sets a limit on the maximum non-inductive plasma current achievable (and on the maximum temperature at fixed current). For this heating mix and for the assumptions made on the density and temperature profiles, 7.4 MA is the maximum current that can be driven

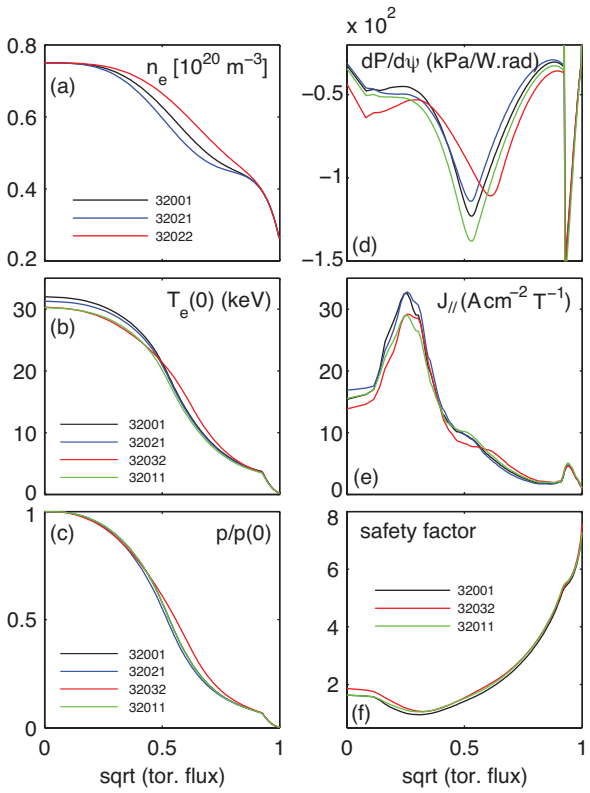


**Figure 8.** (Colour online) Scenarios with 20 MW IC and 40MW EC. (a) Density profiles for the cases with $n(0)/\langle n\rangle = 1.4$ (#32001), $n(0)/\langle n\rangle = 1.3$ (#32021) and $n(0)/\langle n\rangle = 1.5$ (#32022). All other cases use the density profile peaking of #32001. (b) Temperature profiles: #32032 has $\rho_{\rm ITB} = 0.60$, all the others have $\rho_{\rm ITB} = 0.55$. (c) pressure profiles, normalized to the maximum, same cases as in (b). (d) pressure derivative. (e) total parallel current. (f) safety factor profile.

non-inductively without allowing too large of a confinement value.

### *4.2. Configurations with 33 MW of NB, 20 MW of IC and 40 MW of EC.*

Table 3 reports the plasma parameters and the ideal MHD stability results for some of the configurations with 40 MW EC heating analyzed: two cases respectively with more and less peaked density profile, one case with broader temperature profile and one with 10% higher density. The profiles for these cases are compared with those of the reference scenario in Fig.8. The last two columns report two cases with different settings in the ECRH launchers: case #32602 has higher azimuthal angle (41 degrees instead of 40) and #32621 uses two equatorial launchers in the co-current direction (upper and lower) and one of the upper launchers. It is assumed that each launcher carries on 6.5 MW of power. The latter two cases are compared to #32001 in Fig.9.

The total non-inductive current of this heating configuration is strongly sensitive to variations of the density amplitude and peaking factor. While the scenario with broader ITB (#32032) can achieve the same current as the reference scenario, changing

the density peaking factor from 1.4 to 1.3 loses about 150 kA, while increasing the density by 10% results in a loss of about 700 kA of externally driven current, which is not compensated by the gain in bootstrap current (200 kA).
The scenario #32021 has low $H_{98}$ compared to the target value and to the other configurations, which explains the lower non-inductive current.

As shown in Fig.8, the variation in the pressure, current density and safety factor profiles are small and - except for the case with the broadest pressure profile (#32032) - the current density profiles show little variation at radii $\rho > 0.4$.

The relaxed equilibria are unstable to $n = 1$ ideal kinks around the operating point and display mode structure similar to the reference scenario, with dominating higher $m$ harmonics (see Fig.6-d).

The ideal MHD stability is strongly sensitive to the EC heating deposition profile. Increasing the azimuthal angle by only one degree is effective in moving the position of

**Table 3.** Scenarios with 20MW IC and 40MW EC heating. Variations of the reference scenario #32001 for perturbations of the pressure around the operating point. The target current for these scenarios is 9 MA.

| 33 MW NB<br>20 MW IC<br>40 MW EC | 32021 | 32022 | 32032 | 32011 | 32604 | 32621 |
|---|---|---|---|---|---|---|
| $I_{\rm NI}$ (MA) | 8.83 | 8.84 | 9.1 | 8.59 | 8.9 | 8.4 |
| $I_{\rm NB}$ (MA) | 3.0 | 2.75 | 2.96 | 2.4 | 3.1 | 3.0 |
| $I_{\rm BS}$ (MA) | 3.6 | 3.9 | 4.0 | 4.0 | 3.9 | 4.0 |
| $I_{\rm EC}$ (MA) | 1.67 | 1.6 | 1.6 | 1.5 | 1.65 | 1.20 |
| $P_\alpha$ | 48 | 56 | 52 | 60 | 53 | 52 |
| $Q$ | 3.0 | 3.6 | 3.3 | 3.8 | 3.4 | 3.3 |
| $p(0)/\langle p\rangle$ | 2.77 | 2.59 | 2.57 | 2.68 | 2.67 | 2.68 |
| $\mathbf{n(0)}/\langle \mathbf{n}\rangle$ | 1.5 | 1.3 | 1.4 | 1.4 | 1.4 | 1.4 |
| $\mathbf{n(0)[10^{19}m^{-3}]}$ | 7.5 | 7.5 | 7.5 | 8.2 | 7.5 | 7.5 |
| $T_{\rm e}(0)$ (keV) | 31 | 32 | 30 | 30 | 32 | 31 |
| $\rho_{\mathbf{ITB}}$ | 0.55 | 0.55 | 0.60 | 0.55 | 0.55 | 0.55 |
| $\beta_{\rm N}$ | 2.3 | 2.5 | 2.49 | 2.64 | 2.48 | 2.53 |
| $q(0)$ | 1.58 | 1.77 | 1.92 | 1.67 | 2.03 | 1.87 |
| $q_{\rm min}$ | 0.96 | 1.0 | 1.07 | 1.06 | 1.14 | 1.20 |
| $H_{98}$ | 1.52 | 1.62 | 1.61 | 1.61 | 1.60 | 1.63 |
| $n/n_{\rm G}$ | 0.84 | 0.89 | 0.87 | 0.96 | 0.86 | 0.89 |
| ballooning | S | S | S | S | S | S |
| n=1, no wall | U | U | U | U | S | S |
| n=1, wall | U | U | U | U | S | S |

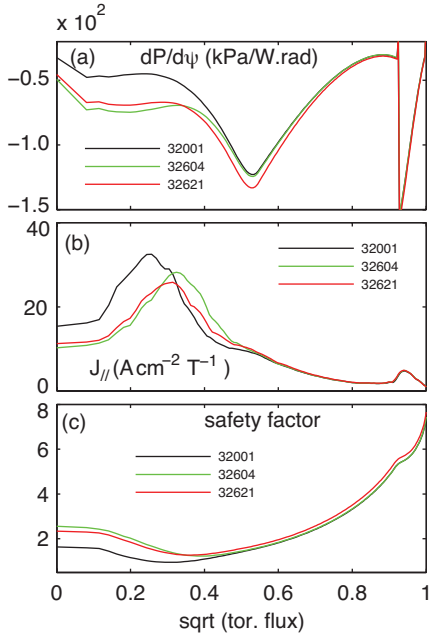


**Figure 9.** (Colour online) Configurations with 40 MW EC. Pressure derivative (a), parallel current density (b) and safety factor (c) profiles of the reference scenario #32001, of a configuration with larger azimuthal angle (#32604) and of a configuration that uses two equatorial launchers in co-current and one upper launcher (#32621).

$q_{\min}$ at larger radii, as shown in Fig.9. This configuration is ideal MHD stable both to $n = 1$ and $n = 2$ kinks without wall.

The above scenarios have been calculated assuming that all three equatorial launchers can inject in the co-current direction, while the ECRH system on ITER will use counter-current injection from the middle equatorial launcher. The results presented here are therefore optimistic for the calculation of the current drive and pessimistic for the ideal MHD stability predictions, since it is expected that with about 2/3 of the current driven by ECRH, $q_{\min}$ will be higher. Using two launchers from the equatorial plane (respectively the top and bottom) and one of the upper launchers loses about 400 kA of ECCD (case #32621 in table 3) and achieves only 8.4 MA of non-inductive current. This configuration, like #32602, has current density profile peaked at larger radii; it has $q_{\min}$ below 1.5 but is MHD stable, suggesting that the position of $q_{\min}$ rather than its value is most important in determining the ideal MHD stability of this heating mix configuration.

### *4.3. Configurations with 33 MW NB, 20 MW EC and 20 MW LH.*

Table 4 reports the plasma parameters and the ideal MHD stability results of some of the analyzed scenarios with 20MW each of EC and LH: a configuration with broader density profile (#33021) and one with $\rho_{\rm ITB} = 0.50$ (#33031) at the reference pressure and three configurations at 10% larger density and with three different $\rho_{\rm ITB}$ values. The

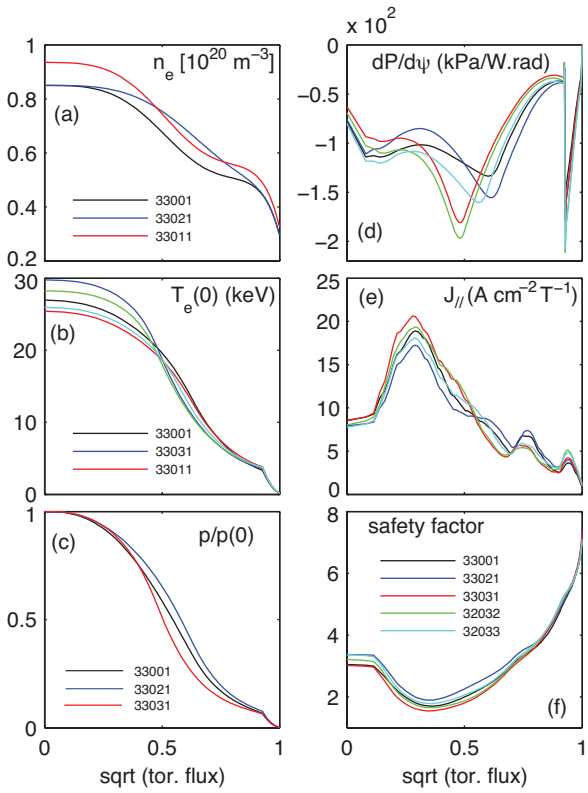


**Figure 10.** (Colour online) Scenarios with EC and LH heating. (a) density profiles for $n(0)/\langle n\rangle = 1.5$ (#33001), $n(0)/\langle n\rangle = 1.3$ (#33021) and for $n(0)/\langle n\rangle = 1.5$ and 10% larger density (#33011). All other cases use the density profile of #33001. (b) Electron temperature profiles. (c) pressure profiles normalized to the maximum, for the reference case and for the cases with most peaked (#33031) and less peaked pressure profile (#33021). (d) pressure derivative, same cases as (b). (e) current density profiles. (f) safety factor profiles.

corresponding profiles are compared to the reference scenario #33001 in Fig.10.

Both the configuration with broader density profile (#33021) and with 10% higher density (#33011) achieve non-inductive current comparable to the reference scenario, while operating with more peaked ITBs increases the driven current by about 100-150 kA.

At the reference pressure the relaxed equilibrium is stable to $n = 1$ kinks even with more peaked ITBs at mid-radius. At higher density the equilibrium is instead unstable to $n = 1$ ideal kinks for ITBs at $\rho_{\rm ITB} = 0.5$ and stable for ITBs at $\rho_{\rm ITB} > 0.6$.

The kink mode structure is similar to that shown in Fig.6 for the scenario #34001 and is not shown here, with a dominant $m = 2$ component and harmonics with $m > 4$ having comparable amplitude. Similarly to #34001, also in this case the maximum pressure gradient in the configuration with ITB at mid-radius is very close to the location of $q_{\rm min}$.

Peaked ITBs, with foot at $\rho_{\rm ITB} \leq 0.5$, make the plasma more unstable also to large-

$n$ ballooning modes; the toroidal mode number of the marginally stable mode decreases from $n_{\rm cr} = 44$ in the reference scenario to $n_{\rm cr} = 20$ in the plasma with more peaked ITB (#33031).

### *4.4. Configurations with 33 MW of NB, 20 MW of IC and 40 MW of LH.*

The ideal MHD stability of this heating mix configuration is qualitatively similar to that of the scenario with EC and LH heating. Table 5 reports selected cases, with $n \leq 1.2 n_{\rm G}$ and ITBs in the range of $\rho_{\rm ITB} = [0.45, 0.70]$.

About 100 kA of non-inductive current are lost when the density is increased by 10%, although most configurations achieve non-inductive currents within 30 kA in excess of $I_{\rm P} = 10$ MA at $H_{98} = 1.57-1.64$. Operating with broader ITBs significantly improves the ideal MHD stability of this configuration. As shown in Fig.11, when the ITB foot is moved outboard (#32031, #32032 and #34035) the current profile broadens and its

**Table 4.** Scenarios with 20MW EC and 20MW LH heating. The target plasma current for these configurations is 8.85 MA.

| 33 MW NB<br>20 MW LH<br>20 MW EC | 33021 | 33031 | 33011 | 33033 | 33032 |
|---|---|---|---|---|---|
| $I_{\rm NI}$ (MA) | 8.8 | 8.82 | 8.87 | 8.82 | 8.87 |
| $I_{\rm NB}$ (MA) | 2.15 | 2.4 | 2.0 | 2.1 | 2.1 |
| $I_{\rm BS}$ (MA) | 5.0 | 4.7 | 5.3 | 5.2 | 5.1 |
| $I_{\rm EC}$ (MA) | 0.73 | 0.80 | 0.70 | 0.70 | 0.73 |
| $P_\alpha$ | 69 | 64 | 73 | 73 | 73 |
| $Q$ | 4.7 | 4.4 | 5.0 | 5.0 | 5.0 |
| $p(0)/\langle p\rangle$ | 2.4 | 2.8 | 2.5 | 2.6 | 2.8 |
| $\mathbf{n(0)}/\langle \mathbf{n}\rangle$ | 1.3 | 1.4 | 1.4 | 1.4 | 1.4 |
| $\mathbf{n(0)[10^{19}m^{-3}]}$ | 8.5 | 8.5 | 9.3 | 9.3 | 9.3 |
| $T_{\rm e}(0)$ (keV) | 26 | 29 | 25 | 26 | 28 |
| $\boldsymbol{\rho_{\rm ITB}}$ | 0.55 | 0.50 | 0.55 | 0.60 | 0.50 |
| $\beta_{\rm N}$ | 2.7 | 2.7 | 2.8 | 2.8 | 2.8 |
| $q(0)$ | 3.3 | 2.8 | 3.6 | 3.4 | 3.4 |
| $q_{\rm min}$ | 1.89 | 1.53 | 1.80 | 1.80 | 1.69 |
| $H_{98}$ | 1.65 | 1.64 | 1.64 | 1.64 | 1.65 |
| $n/n_{\rm G}$ | 1.0 | 0.96 | 1.05 | 1.05 | 1.05 |
| ballooning | U | U | U | U | U |
| n=1, no-wall | S | S | S | S | U |
| n=1 wall | S | S | S | S | S |

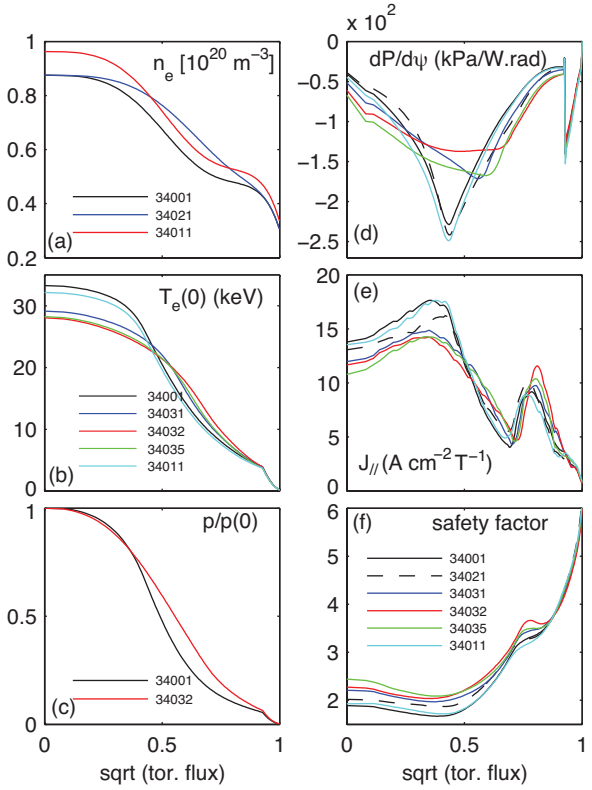


**Figure 11.** (Colour online) Scenarios with 20 MW IC, 40MW LH and 33 MW of NB. (a) density profiles. (b) electron temperature profiles. (c) pressure profiles, normalized to the maximum, for the cases with the largest and the lowest pressure peaking factor. (d) pressure derivative. (e) parallel current density. (f) safety factor.

maximum decreases causing $q_{\min}$ to increase above 2. Second, the pressure gradient at the ITB location decreases and its maximum moves outboard, far from the $q_{\min}$ radius, removing the driving mechanism for ideal kinks at large $\beta_{\rm N}$ and a seed to the $(2,1)$ infernal mode.

Figure 12 reports the solutions of the ballooning equation as a function of the ITB foot location, after profile relaxation. The ballooning eigenvalues $\omega^2$ monotonically decrease in absolute value with increasing $\rho_{\rm ITB}$ and the radial extent of the unstable region decreases from about 20% of the minor radius with the most peaked ITB to about 10% for $\rho_{\rm ITB} = 0.60$. The toroidal mode number of the marginally unstable mode rapidly increases and becomes larger than 50 when $\rho_{\rm ITB} \geq 0.6$; the equilibrium becomes stable when $\rho_{\rm ITB} > 0.65$.

### *4.5. Configurations with 8 MW of NB, 20 MW of IC and 40 MW of LH.*

This configuration suppresses the NB driven current to produce a significantly different $q$ profile. As shown in Fig.13, perturbations in the density peaking have a major effect on the total non-inductive current and on the safety factor profile of this heating mix configuration: when $n(0)/\langle n\rangle$ is changed from 1.3 to 1.4 both the NB and the LH

current drive increase by about 200-250 kA and the bootstrap current from 4.9 to 5.3 MA, bringing the total non-inductive current from 7.25 to 8.15 MA and raising the fusion gain factor from 2.4 to 3.14. As shown in Fig.13, $q_{\min}$ decreases from 4.5 to 3.5, faster than the $q(0)$ decrease, resulting in a stronger sheared profile near the core. The various equilibria remain ideal MHD stable, although fast ion driven instabilities might be an issue at these values of $q$ [13].

## 5. Non relaxed configurations

This section discusses how the safety factor profile affects the ideal MHD stability in the flat-top, when the current profiles have not yet reached a relaxed state. The day one heating mix configuration and the scenario with 8 MW of NB, which are stable throughout the flat-top phase, are not included in the discussion.
It was previously shown (see Fig.3-c) that in all configurations with 33 MW of NB the safety factor reaches large values on axis before relaxing to its stationary values. It will

**Table 5.** Scenarios with 20MW IC, 40MW LH and 33MW NB heating. The target current is 10 MA.

| 33 MW NB<br>20 MW IC<br>40 MW LH | 34021 | 34031 | 34032 | 34011 | 34035 |
|---|---|---|---|---|---|
| $I_{\rm NI}$ (MA) | 9.68 | 10.1 | 10.3 | 9.9 | 10.2 |
| $I_{\rm NB}$ (MA) | 2.5 | 2.6 | 2.6 | 2.3 | 2.3 |
| $I_{\rm BS}$ (MA) | 5.2 | 5.3 | 5.4 | 5.5 | 5.9 |
| $P_\alpha$ | 83 | 74 | 74 | 87 | 87 |
| $Q$ | 5.3 | 4.8 | 4.7 | 5.5 | 5.6 |
| $p(0)/\langle p\rangle$ | 2.7 | 2.6 | 2.5 | 2.5 | 2.6 |
| $\mathbf{n(0)}/\langle \mathbf{n}\rangle$ | 1.4 | 1.5 | 1.4 | 1.4 | 1.4 |
| $\mathbf{n(0)[10^{19}m^{-3}]}$ | 8.7 | 8.7 | 8.7 | 9.6 | 9.6 |
| $T_{\rm e}(0)$ (keV) | 32 | 29 | 28 | 32 | 28 |
| $\rho_{\mathbf{ITB}}$ | 0.45 | 0.6 | 0.7 | 0.45 | 0.65 |
| $\beta_{\rm N}$ | 2.9 | 2.6 | 2.6 | 2.86 | 2.8 |
| $q(0)$ | 1.78 | 2.2 | 2.3 | 1.95 | 2.45 |
| $q_{\min}$ | 1.77 | 1.97 | 2.04 | 1.72 | 2.09 |
| $H_{98}$ | 1.64 | 1.58 | 1.57 | 1.64 | 1.62 |
| $n/n_{\rm G}$ | 0.90 | 0.84 | 0.84 | 0.93 | 0.92 |
| ballooning | U | U | S | U | S |
| n=1, no-wall | U | S | S | U | S |
| n=1 wall | S | S | S | S | S |

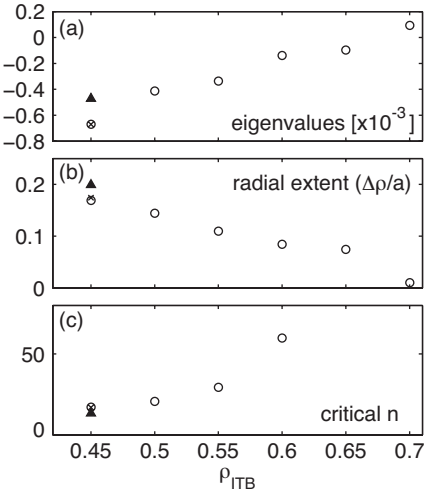


**Figure 12.** Scenario with IC, LH and 33MW NB. Solutions of the ideal ballooning equation at the reference pressure (○) as a function of the ITB foot location. Also shown are the values for density peaking 1.3 (▲) and for 10% higher density (×). (a) eigenvalues $\omega^2$ of the most unstable mode, (b) radial extension of the unstable region, as a fraction of the minor radius, (c) toroidal mode number of the marginally unstable mode.

be shown in this section that, during the first part of the flat-top phase, typically for $t < 600$s when the magnetic shear is strongly reversed in the core, the plasma is stable to $n = 1$ kinks and to large-$n$ ballooning instabilities. For later times, it is observed that configurations with LH heating in particular (combined with either EC or IC) are sensitive to the value of $q_{\min}$: both ballooning and kink instability is better in the first third of the flat-top phase, when the minimum safety factor is typically close to or above 2.

### *5.1. Configurations with 33 MW of NB, 20 MW of IC and 40 MW of EC.*

Figure 14 shows the profiles of safety factor, pressure derivative and total parallel current in the case of the reference scenario, #32001, calculated at four time slices during the flat-top phase, as well as the Fourier harmonics of the $n = 1$ ideal kink calculated at 800s.

The equilibrium is ideal MHD unstable with wall for $t \geq 800$s and stable without wall at earlier times. As shown in Fig.14, the current density profile is stiff for $\rho \geq 0.6$ and so are the pressure profiles (we remind that in these simulations the density profiles and the pedestal temperature are prescribed). The $J_{\|}$ profile, which is peaked at $\rho \simeq 0.35$ at 700s and 800s, shifts inward at later times and peaks at $\rho \simeq 0.25$ in the relaxed phase. As discussed in Sec.4.2, current profiles peaked at larger radii lead to more stable configurations. Although $q_{\min} < 1.5$ both at 700s and at 800s, the plasma is stable to $n = 2$ kinks without a wall. At 700s, where the reversed shear in the core is stronger, the plasma is also stable to the $n = 1$ mode. A comparison with Fig.6-d

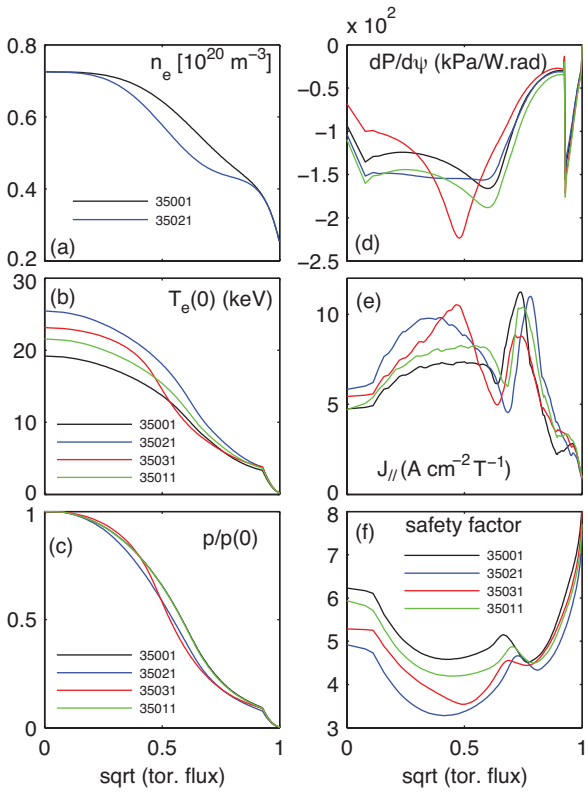


**Figure 13.** (Colour online) Scenarios with 20 MW IC, 40 MW LH and 8 MW of NB. (a) density profiles. (b) electron temperature profiles. (c) pressure profile, normalized to the maximum. (d) pressure derivative. (e) parallel current density. (f) safety factor.

shows that harmonics with low $m$ have larger amplitude, a feature typical of profiles with strong reversed shear in the core [12]. The edge mode structure is instead similar, with dominant, higher-$m$ harmonics at larger radii, a feature justified by similar edge current profiles. The other scenarios with the same heating source combination have features qualitatively similar to the reference scenario.

### *5.2. Configurations with 33 MW NB, 20 MW EC and 20 MW LH.*

The ideal MHD stability of this heating mix combination is sensitive to the reverse shear in the core, to the values of $q_{\min}$ and to its radial position relative to the ITB foot. The most stable equilibria have strong reverse shear in the core and $q_{\min} > 2$, two conditions that are typically satisfied in the first third of the flat-top phase. The most unstable equilibria are those where the maximum ITB pressure gradient is close to $\rho(q_{\min})$ and to the $q = 2$ rational surface.

Figure 15 shows the profiles of pressure derivative, total parallel current and safety factor calculated at four time slices in the flat-top phase, in the case of the reference scenario (#33001) and for two of the configurations listed in table 4: the scenario with ITB at mid-radius (#33031) and the scenario with 10% higher density and ITB at

mid-radius (#33032).

The reference scenario is stable to $n = 1$ kinks without wall throughout the flat-top phase. The pressure and current profiles display little variation outside $\rho \sim 0.5$ and the maximum current density profile peaks at the same radial location during most of the flat-top phase. With ITBs at 1/2 of the minor radius (#33031) equilibria are unstable without wall to $n = 1$ kinks in a limited time window $t = [700, 900]$s, where $q_{\min} \sim 1.6 - 1.7$. As shown in Fig.15, the ITB pressure gradient is higher in this plasma that in the reference scenario and it peaks close to the minimum safety factor. At $t > 900$s, where the current peaks more inward (and the ITB foot and $\rho(q_{\min})$ are more apart from each other) equilibria are stable.

The last case (#33032) has also ITB at mid-radius, but higher density. The ITB pressure gradient is therefore slightly larger than the previous case and $\beta_{\rm N} = 2.8$ compared to $\beta_{\rm N} = 2.7$. This configuration is unstable to the $n = 1$ without wall, but stable with wall, at all times.

The other scenarios listed in table 4 and not shown in Fig.15 have similar profiles

**Table 6.** Scenarios with 20MW IC, 40MW LH and 8MW NB heating. The target current is 7.5 MA.

| 8 MW NB<br>20 MW IC<br>40 MW LH | 35021 | 35031 | 35011 |
|---|---|---|---|
| $I_{\rm NI}$ (MA) | 8.3 | 7.6 | 8.1 |
| $I_{\rm NB}$ (MA) | 0.76 | 0.65 | 0.5 |
| $I_{\rm BS}$ (MA) | 5.3 | 4.9 | 5.6 |
| $P_\alpha$ | 43 | 40 | 48 |
| $Q$ | 3.1 | 2.9 | 3.5 |
| $p(0)/\langle p\rangle$ | 2.6 | 2.5 | 2.3 |
| $\mathbf{n(0)/\langle n\rangle}$ | 1.4 | 1.3 | 1.3 |
| $\mathbf{n(0)[10^{19}m^{-3}]}$ | 7.2 | 7.2 | 8.0 |
| $T_{\rm e}(0)$ (keV) | 25 | 23 | 21 |
| $\rho_{\mathbf{ITB}}$ | 0.65 | 0.5 | 0.65 |
| $\beta_{\rm N}$ | 2.3 | 2.3 | 2.4 |
| $q(0)$ | 4.9 | 5.1 | 6.1 |
| $q_{\min}$ | 3.3 | 3.5 | 4.2 |
| $H_{98}$ | 1.59 | 1.58 | 1.60 |
| $n/n_{\rm G}$ | 0.87 | 0.98 | 1.04 |
| ballooning | S | S | S |
| n=1, no-wall | S | S | S |
| n=1 wall | S | S | S |

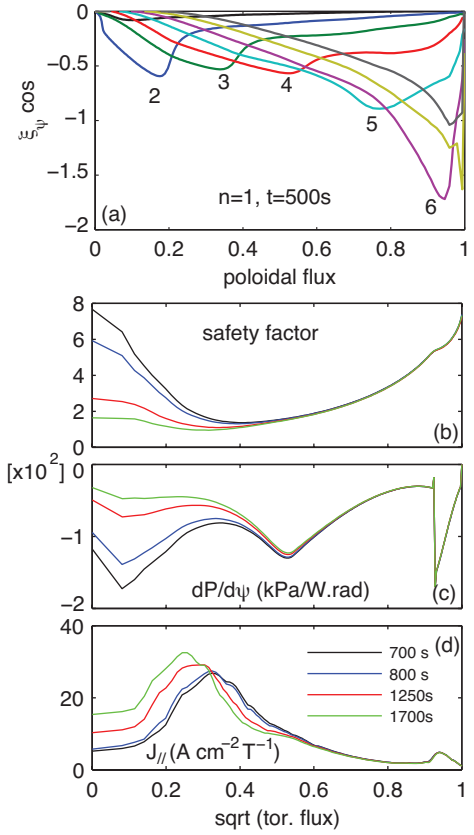


**Figure 14.** (Colour online) Configuration with 40 MW of EC heating, reference scenario #32001. (a) Fourier components of the $n = 1$ ideal kink, calculated at 800s. (b) safety factor profiles calculated at four time slices during the flat-top phase, (c) pressure derivative, (d) total parallel current.

and ideal MHD stability as the reference scenario #33001. They operate with ITBs at $\rho_{\rm ITB} \geq 0.55$ and are stable to ideal $n = 1$ kinks without wall at the base pressure and at 10% larger density at all times.

The results of the ballooning stability analysis are summarized in the last column of Fig.15. Peaked ITBs make the plasma more unstable to large-$n$ ballooning modes: the growth rate of the most unstable mode rapidly increases progressing through the flat-top and saturates when a steady state regime is reached, while the toroidal mode number of the marginally unstable modes decreases to $n_{\rm cr} \sim 20$. It should be noted that plasmas with peaked ITBs also display the larger range of variation in $q_{\rm min}$ and thus the larger stability variation. Since $q_{\rm min}$ decreases during the current flat-top phase, more stable equilibria - found at earlier times - are those associated with larger values of $q_{\rm min}$, as shown in Fig.15-f.

### *5.3. Configurations with 33 MW of NB, 20 MW of IC and 40 MW of LH.*

The stability of this heating mix configuration is qualitatively similar to that of the scenario with EC and LH heating discussed in the previous section. Equilibria are more

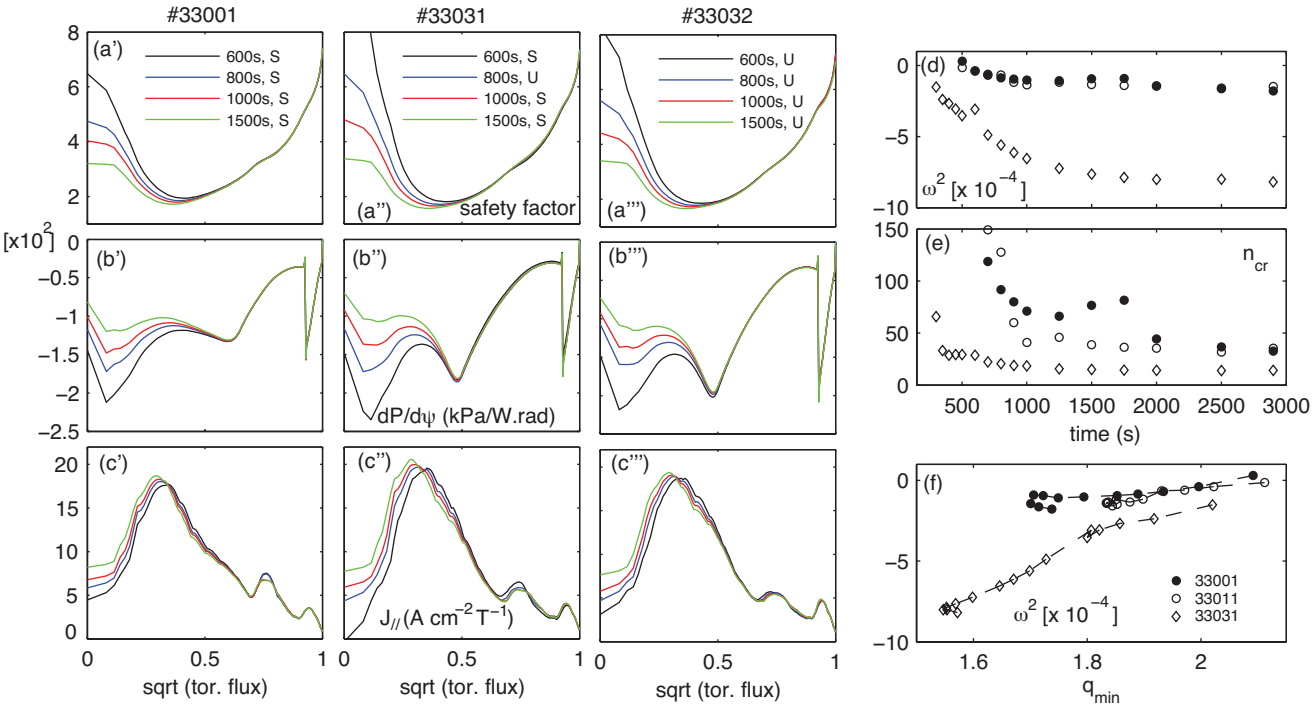


**Figure 15.** (Colour online) Configurations with EC and LH heating. (a) Safety factor profile, (b) pressure derivative, (c) parallel current density profiles, calculated at four time slices during the flat-top phase. For each time it is noted whether the plasma is stable (S) or unstable (U) to $n = 1$ kinks. (d) ballooning eigenvalues calculated during the flat-top phase, for the reference scenario (•), for ITB at $\rho = 0.50$ (◊) and for density increased by 10% (○). (e) critical toroidal mode number $n_{\rm cr}$ of the marginally unstable mode. (f) evolution of the eigenvalues as a function of $q_{\rm min}$ in the flat-top phase.

stable to both ballooning and $n = 1$ ideal kinks in the first third of the flat-top phase, where $q_{\rm min} \geq 2$ and the safety factor on axis is larger.

Figure 16 shows the profiles for the reference scenario (#34001) and for two scenarios with the same density profiles but broader ITBs, with $\rho_{\rm ITB} = 0.55$ (#34031) and $\rho_{\rm ITB} = 0.60$ (#34032).

As shown in the figure, the ITB foot location almost coincides with the radius of the minimum safety factor at all times, which makes this configuration unstable to $n = 1$ kinks without wall for $t \geq 600$s.

The two configurations with broader ITBs are stable to $n = 1$ kinks without wall throughout the flat-top phase, both at the reference pressure and at higher densities.

Equilibria are unstable to large-$n$ ballooning modes throughout the flat-top phase. The variation of the ballooning eigenvalues with time and with $q_{\rm min}$ is reported in the last column of Fig.16 for the reference scenario and for the cases with broader density profile (#34021), broader ITB (#34031) and with 10% higher density (#34011). The growth rate of the most unstable mode increases in absolute value with decreasing $q_{\rm min}$ and equilibria become more stable to ballooning modes when $q_{\rm min} \gtrsim 2$ .

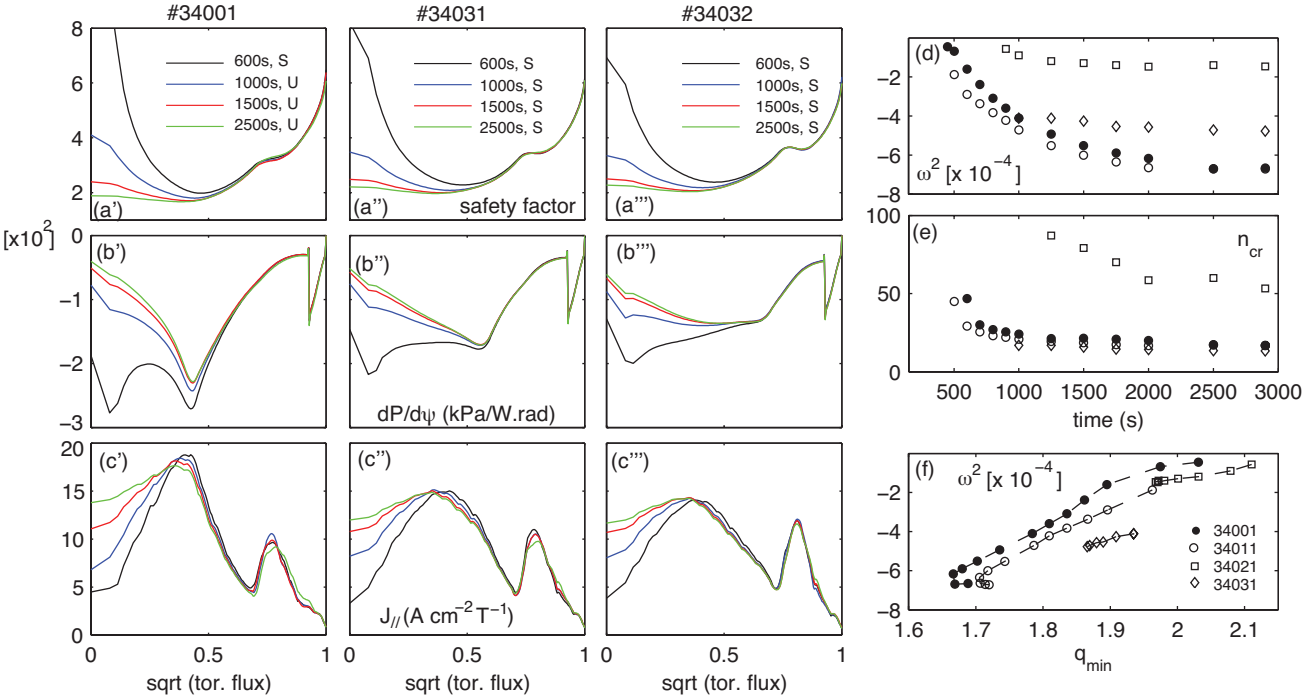


**Figure 16.** (Colour online) Scenario with IC, LH and 33 MW NB. (a) Safety factor profile, (b) pressure derivative, (c) parallel current density profiles, calculated at four time slices during the flat-top phase. For each time it is noted whether the plasma is stable (S) or unstable (U) to $n = 1$ kinks. (d)-(e) Solutions of the ballooning equation calculated for the reference scenario (•), for broader density profile (◇), for ITB at $r/a = 0.60$ (□) and for central density 10% larger (○). (c) dependence of the eigenvalues $\omega^2$ on $q_{\min}$.

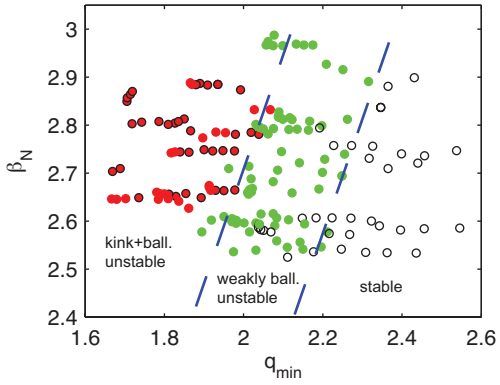


**Figure 17.** (Colour online) $(\beta_{\rm N}, q_{\min})$ space covered during the flat-top phase, for all the configurations with IC and LH heating analyzed. Empty symbols indicate ideal MHD stable equilibria, red symbols indicate ballooning instability and black indicate equilibria unstable to $n = 1$ kinks without the wall. Green indicates weakly ballooning unstable equilibria, typically with critical mode numbers above 40 and radial extent below 10% of the minor radius.

The results from the ideal MHD stability analysis throughout the flat-top, between 350s and 3000s, are summarized in Fig.17, which reports the range of variation of $\beta_N$ and $q_{min}$ for 18 plasma configurations with this same heating mix, including a scan in $\rho_{ITB}$ at the base pressure and at 10% and 20% larger densities, between $0.85n_G$ and $n_G$. Empty symbols indicate ideal MHD stable equilibria, red symbols indicate ballooning instability, black bordered symbols indicate equilibria unstable to $n = 1$ kinks without the wall and stable with wall. None of the analyzed equilibria was found to be unstable to $n = 1$ kink modes with wall. Green symbols indicate weakly ballooning unstable equilibria, typically with critical mode numbers above 50 and radial extent below 10% of the minor radius.
Stability progressively improves with increasing $q_{min}$ and the plasma becomes stable to kink modes when $q_{min} > 2$, although residual ballooning instabilities remain. For $q_{min} > 2.2$ equilibria are ideal MNHD stable. When $q_{min} \geq 2.2$ the equilibria become ideal MHD stable.

## 6. Operational limits

Figure 18 summarizes the results of the ideal MHD stability analysis for all the relaxed configurations analyzed, in three plots of $\beta_N$ as a function of $q_{min}$ (a), of the pressure peaking factor (b) and of the internal inductance (c). Additional configurations at densities up to $\sim 1.2n_G$ and $\rho_{ITB} = [0.50, 0.65]$ have been included in this database for the two configurations with EC+LH and with IC+LH at large NB power.

Data refers to the ideal MHD stability calculated in the relaxed phase and assuming a wall at infinity. Open symbols indicate ideal MHD stable equilibria, while black symbols indicate configurations that are both ballooning and kink unstable and that are not stabilized by the ITER conforming wall. The latter group is limited to plasmas with 40 MW of EC heating with deposition peaked at $\rho < 0.35$. Red and green symbols indicate equilibria that are ballooning unstable, respectively with $n_{cr} < 50$ and with $n_{cr} > 50$, the second group being characterized by a radial extent typically below 10% of the minor radius. This separation is somewhat arbitrary; however, since this data represents the stability at the end of the burning phase, conclusions do not change for different choices of the $n_{cr}$ threshold. Equilibria that are both ballooning and kink unstable without a wall, but stabilized by an ideal wall, are indicated as red symbols with a black border.

Scenarios with IC+EC heating have $q_{min} < 1.5$ in the relaxed flat-top phase and large internal inductance. Adding 20 MW of LH off-axis elevates $q_{min}$ above 1.5 and brings the internal inductance down to $\sim 0.8$. Scenarios with LH heating achieve larger values of $\beta_N$ and can operate above the no-wall limit with an ideal wall. Additional analysis of the resistive wall mode stability is required to determine the long time stability of these configurations. Raising $q_{min}$ above 2 significantly improves the stability, a situation that can be realized by operating with broad pressure profiles, as shown in Fig.18-b, where the green symbols are concentrated in the region of lower pressure

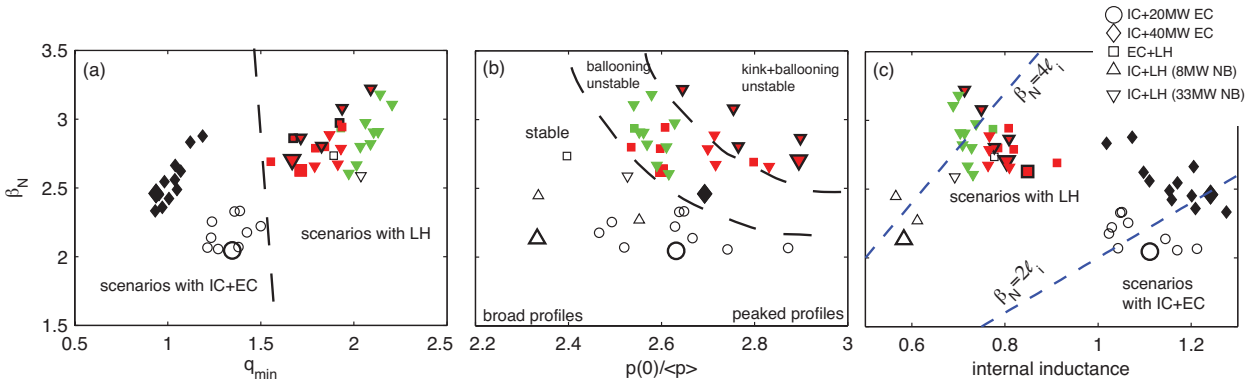


**Figure 18.** (Colour online) (a) Normalized pressure vs minimum safety factor for all scenarios with 33 MW beam heating. The large $q$ configurations with 8 MW and 16 MW of NB are not reported in this figure. (b) Normalized pressure vs pressure peaking factor. For the configurations with 40MW of EC only the reference case is reported in this figure. (c) Normalized pressure vs internal inductance. Open symbols indicate ideal MHD stable equilibria, red and green symbols indicate equilibria unstable to ballooning modes with $n_{cr}$ - respectively - smaller and larger than $n_{cr} = 50$. Kink unstable plasmas are red with black border when stabilized by the wall, black when not stabilized.

peaking factors. The improvement in the MHD stability at low peaking factors is a well known result, both from theory (see Chap.3 in the progress of ITER Physics Basis [12] and references therein) and from experiments [10]. Compared to Fig.10 in Ref.[10], which reports transient and stationary discharge performance in reversed shear plasmas from ASDEX-U, DIII-D, JT-60U and JET, our simulations fall in the low peaking region, although our stability boundary appears shifted towards the left, *i.e.* for the same peaking factor we find that the maximum achievable $\beta_N$ is lower. The different plasma shape is likely a reason for this discrepancy. Most of the database at high $\beta_N$ in Ref.[10] is from DIII-D, where high performance has been transiently achieved operating with strongly shaped plasmas. More recent experiments with ITBs on JT-60U have found values of $\beta_N \simeq= 2.7 - 3.0$ comparable with the limits found herein, operating with similar plasma shape and comparable pressure peaking factors [47][48].

## 7. Conclusions

Non-inductive advanced scenarios in ITER will need to operate with ITBs at normalized pressures close to the ideal no-wall limits, in order to achieve $H_{98} \simeq 1.6$ and $Q > 5$ at a plasma current of 9 MA [2][3][11]. In this work we have discussed the ideal MHD stability and the operational limits of steady state configurations with different combinations of heating and current drive sources: IC with EC, LH with IC and LH with EC, all combined with additional NB. Combined with about 50% of self-driven bootstrap current, these sources can deliver between 7 and 10 MA of plasma current. For these heating configurations, we have defined a range of flat-top equilibria that are

stable against ideal MHD instabilities and discussed the effect of the various heating sources on the steady-state equilibria.

It is found that 73 MW of heating power (20 MW each of IC and EC combined with 33 MW NB), as planned for the initial operations on ITER, can deliver up to 7.4 MA of non-inductive current in the flat-top. Although this scenario has low fusion gain and it operates at $\beta_N \lesssim 2.4$, it is predicted to be ideal MHD stable for variations of the plasma parameters around the operating point. It would be therefore a good candidate to demonstrate the feasibility of steady-state, stable operations at moderate $\beta_N$, with densities close to the Greenwald limit.

Different options are under consideration for the upgrade of the heating system on ITER, including doubling the EC power and adding up to 40 MW of LH [43]. The stability of configurations with 40 MW EC power is found to be sensitive to the position of $q_{\min}$, which is controlled by the heating deposition profile. Equilibria stable to $n = 1, 2$ kinks without wall exist even with $q_{\min} < 1.5$, provided the EC heating deposition profiles peak at $\rho \geq 0.35$.

With almost the same non-inductive current delivered, a combination of 20 MW each of EC and LH has better performance and ideal MHD stability than a combination of 20 MW of IC and 40 MW of EC. Lower Hybrid heating is favorable to maintain the minimum safety factor above 1.5, which is desirable in steady state operations to avoid Neoclassical Tearing Modes with $(m, n) = (3, 2)$, but can only dominate the current profile when it is coupled to low beam power. Configurations with LH heating (combined with EC or with IC) can achieve $\beta_N \sim 4\ell_i$ operating with ITBs at 2/3 of the minor radius. Operating with broad pressure profiles improves significantly the MHD stability, rising the safety factor above $q_{\min} > 2$ and moving the ITB pressure gradient away from the minimum of $q$. These equilibria are computed to be weakly unstable to ballooning modes in ideal MHD, but we expect them to be stabilized by non-ideal effects.

In absence of a reliable transport model, the simulations presented in this work use a semi-empirical model for internal barriers in the electron and ion temperature. Like most simulations of steady state scenarios, where hypotheses are made on the density and temperature profiles and on the transport model, a benchmark against experiments is missing. Although the ITB parameters have been chosen to be consistent with the available database for reversed shear plasmas, mainly from JT-60U, a direct comparison with experiments on present devices, with moderate transport barriers and intermediate plasma shape ($\delta \simeq 0.4 - 0.45$) is deemed necessary for reliable projections to ITER plasmas.

## Acknowledgments

F. Poli acknowledges J. Chen for help with TSC, C. Ludescher-Furth, D. McCune and T. Rafiq for help with TRANSP. The opinions expressed herein do not necessarily state or reflect those of the ITER organization. This work was supported by the US Department

of Energy under contract DE-AC02-CH0911466.

[1] ITER Physics Basis, Nucl. Fusion (1999) **39**, Progress in the ITER Physics Basis, Nucl. Fusion (2007) **47**.
[2] Shimomura *et al*, Plasma Phys. Control. Fusion **43** (2001) A385
[3] Green BJ Plasma Phys. Control. Fusion (2003) **45** 687-706
[4] Gormezano C. *et al*, in Progress in the ITER Physics Basis, Nucl. Fusion (2007) **47** S285
[5] Joffrin E, Plasma Phys. Control. Fusion **49** (2007) B629
[6] Kessel CE, et al, Nucl. Fusion (2009) **49** 085034
[7] Kessel CE *et al*, Nucl. Fusion (2007) **47** 1274
[8] Bickerton RJ *et al*, (1971) Nature Phys. Sci. **229** 110
[9] Troyon F *et al*, Plasma Phys. Control. Fusion (1984) *26* 209
[10] Sips ACC, Plasma Phys. Control. Fusion (2005) **47** A19
[11] Litaudon X, 2006 Plasma Phys. Control. Fusion **48** A1-A34
[12] Hender TC *et al*, in Progress in the ITER Physics Basis, Nucl. Fusion (2007) **47** S155
[13] Zonca F *et al*, Plasma Phys. Control. Fusion (2006) **48** B15-28
[14] Manickam J *et al*, *Proc. 16th International Conference on Fusion Energy* (Montreal, Canada, 1996) (Vienna: IAEA), F1-CN-64/A5-2
[15] Takeji S *et al* (2002) **42** 5
[16] Huysmans GTA *et al* Nucl. Fusion (1999) **39** 1489
[17] Hender TC *et al* Plasma Phys. Control. Fusion (2002) **44** 1143
[18] Turnbull AD *et al* (2002) **42** 917
[19] Günter S *et al* Nucl. Fusion (2000) **40** 1541
[20] Kamada Y, Plasma Phys. Control. Fusion **42** (2000) A65
[21] Turnbull AD *et al*, Nucl. Fusion (1998) **38** 1467
[22] Lin-Liu YR *et al*, Phys. Plasmas (1999) **6** 3934
[23] Garofalo AM *et al*, Phys. Plasmas (2006) *13* 056110
[24] Jardin SC *et al*, (1986) J. Comput. Phys. **66** 481.
[25] Hawryluk RJ (1980) An empirical approach to tokamak transport *Physics close to thermonuclear conditions* vol.1, ed. B. Coppi *et al* (Brussels: Commission of the European Communities) p.19 TRANSP web site: http://w3.pppl.gov/transp
[26] Snyder P *et al*, Nucl. Fusion (2009) **49** 085035
[27] Gohil P *et al*, Nucl. Fusion (2003) **43** 708
[28] Tang WM, Nucl. Fusion (1986) **26** 1605
[29] Kessel CE *et al*, *Development of the ITER Advanced Steady State and Hybrid Scenarios*, IAEA Fusion Energy Conference 2010, South Korea.
[30] Kikushkin AS et al, Nucl. Fusion (2007) **47** 698
[31] Rafiq T *et al*, *IFP-CNR - Chalmers Workshop on Nonlinear Phenomena in Fusion Plasmas*, AIP Conf. Proc. 1392, 92-100 (2011)
[32] Brambilla M, (1996) A full Wave code for Ion cyclotron waves in toroidal plasmas, Rep. IPP 5/66, Max-Planck-Institut fur Plasmaphysik, Garching
[33] Goldston, RJ *et al*, J. Comput. Phys. (1981) **43** 61
[34] Pankin A *et al*, Comput. Phys. Commun (2004) **159** 157
[35] Ignat DW *et al* 1994 *Nucl. Fusion* **34** 837
[36] Harvey RW and McCoy MG, Proceedings of the IAEA Technical Committee on Advances in Simulation and Modeling of Thermonuclear plasmas, Montral, Quebec (International Atomic Energy Agency, Vienna, 1993), p. 489
[37] Kritz AH *et al*, *Heating in Toroidal plasmas*, Proc. 3rd Joint Varenna-Grenoble Int. Symp. (Grenoble, 1982) vol 2 (Brussels: CEC), page 707.
[38] Lin Liu YR, Chan VS and Prater R, (2003) Phys. Plasmas **10** 4064
[39] DeLucia J, Jardin SC and Todd AMM, J. Comput. Physics (1980) **37** 183
[40] Grimm RC, Greene JM and Johnson JL, Methods Comput. Phys. (1976) **16** 253

[41] Green JM and Chance MS, Nucl. Fusion (1981) **21** 453
[42] Chance MS, Kessel C and Jardin SC, Plasma Phys. Control. Fusion (1999) **44** 1379
[43] Bora D, Beaumont B, Goulding R, Jacquinot J, Kobayashi N, Swain D and Tanga A, in *Radio Frequency Power in Plasmas: 17th Topical Conference on Radio Frequency Power in Plasmas*, edited by P.M. Ryan and D.A. Rasmussen, AIP (2007) **933** 25
[44] Sauter O and Angioni C, Phys. Plasmas (1999) **6** 2834
[45] Houlberg WA *et al*, Phys. Plasmas (1997) **4** 3230
[46] Manickam J, Pomphrey N and Todd AM, Nucl. Fusion (1987) **27** 1461
[47] Takenaga and the JT-60U team, Nucl. Fusion (2007) **47** S563-S578
[48] Oyama N and the JT-60U team, Nucl. Fusion (2009) **49** 104007

The Princeton Plasma Physics Laboratory is operated
by Princeton University under contract
with the U.S. Department of Energy.

Information Services
Princeton Plasma Physics Laboratory
P.O. Box 451
Princeton, NJ 08543

Phone: 609-243-2245
Fax: 609-243-2751
e-mail: pppl_info@pppl.gov
Internet Address: http://www.pppl.gov